

DCText: Scheduled Attention Masking for Visual Text Generation via Divide-and-Conquer Strategy

Jaewoo Song^{1,2}Jooyoung Choi¹Kanghyun Baek³Sangyub Lee³Daemin Park¹Sungroh Yoon^{1,3,4,*}¹Department of Electrical and Computer Engineering, Seoul National University²Global Technology Research, Samsung Electronics³IPAI, ⁴AIIS, ASRI, INMC, ISRC, Seoul National University

{woo.song, jy.choi, qor6271, nickyub, eoalsqkr12, sryoon}@snu.ac.kr



Figure 1. Given a global prompt and target regions (red boxes), DCText decomposes the target text (highlighted in red) and assigns it to regions, enabling accurate and coherent visual text generation, which the base Flux [15] model struggles to handle reliably. The prompts below each image are abbreviated from the original global prompts (full prompts in Appendix E.3).

Abstract

Despite recent text-to-image models achieving high-fidelity text rendering, they still struggle with long or multiple texts due to diluted global attention. We propose DCText, a training-free visual text generation method that adopts a divide-and-conquer strategy, leveraging the reliable short-text generation of Multi-Modal Diffusion Transformers. Our method first decomposes a prompt by extracting and dividing the target text, then assigns each to a designated region. To accurately render each segment within their regions while preserving overall image coherence, we introduce two attention masks—Text-Focus and Context-Expansion—applied sequentially during denoising. Additionally, Localized Noise Initialization further improves text accuracy and region alignment without increasing computational cost. Extensive experiments on single- and multi-sentence benchmarks show that DCText achieves the best text accuracy without compromising image quality while also delivering the lowest generation latency.

1. Introduction

Visual text generation has consistently been a challenging task within the text-to-image (T2I) [10, 15, 24, 29, 31] domain. Despite the impressive image quality of early T2I models, they still struggle to generate accurate and natural-looking visual text. While many methods [5, 17, 18, 32, 40] attempt to overcome this limitation by adding auxiliary modules or fine-tuning, they are often constrained by the capacity of the base model, resulting in poor quality.

Recently, Multi-Modal Diffusion Transformer (MM-DiT) models such as Stable Diffusion 3 series [10] and Flux [15], equipped with powerful text encoders [26], have significantly improved text rendering capabilities inherently. Building on this, several approaches [8, 13] directly leverage them as backbones in a training-free manner to improve visual text generation. However, these methods still introduce inference-time computational overhead and lack sufficient text accuracy. In particular, the latter issue primarily stems from the global attention mechanism: as the amount of text to be rendered increases, the full attention structure in MM-DiT—where all text and image tokens mutually attend to one another—dilutes attention to individ-

*Correspondence to: Sungroh Yoon (sryoon@snu.ac.kr)

ual text tokens, thereby causing omissions, typos, and misplacements that degrade the overall text fidelity.

In this paper, we introduce DCText, which addresses the limitations of the full attention by applying scheduled attention masking to ensure accurate text generation at specified positions. Our method builds on the observation that Flux can reliably produce relatively short, single pieces of text with high fidelity. Leveraging this, we adopt a divide-and-conquer strategy: a global prompt containing multiple or lengthy rendering texts is decomposed into partial prompts based on its text content. Each partial prompt is then responsible for generating its assigned text within a designated region, while the overall image remains consistent with the global prompt. This divide-and-conquer generation is implicitly carried out within a single denoising process, enabled solely by attention masking. However, this approach requires careful mask design, as the split text segments belong to both partial and global prompts, increasing the risk of duplicated text generations, and the image regions generated by these separated prompts often struggle to blend seamlessly with the surrounding background.

To address these challenges, we design two attention masks. *Text-Focus Attention Mask*: concentrates attention into each designated region, ensuring that the generated text is accurate and confined to the target region without duplication. *Context-Expansion Attention Mask*: allows bidirectional interactions between each region and its surrounding background, enabling smooth and coherent transitions across boundaries. By sequentially applying these masks during the denoising process, our method balances accurate text fidelity and visual coherence in the final output. In addition, we propose a *Localized Noise Initialization* approach, which refines the initial noise to provide spatial guidance for the text to be rendered in each region. This approach is not only computationally efficient but also improves region-text alignment and enhances the text accuracy.

We evaluate DCText on diverse datasets containing both single and multiple rendering sentences. Our method achieves the highest text accuracy among other tuning-free approaches, while also delivering the best image quality. Remarkably, these results are obtained with the fewest denoising steps and the lowest latency, and DCText further provides flexible controllability over text placement.

2. Related Work

2.1. Visual Text Generation

With advances in text-to-image models, various methods have been proposed to generate images containing text. Some approaches train character-level text encoders [17–19, 35, 36, 42], enabling models to recognize and generate glyph structures at the character level. Others incorporate external modules into T2I models [5, 6, 21, 32–34, 40, 41]

to handle glyph-level information, which not only improves text rendering accuracy but also enables spatial control over text layout through masks or region-based guidance. However, these methods are built upon U-Net-based Stable Diffusion models [30] and often require additional training, exhibiting limitations in both visual fidelity and text accuracy.

To overcome these challenges, recent research has focused on training-free approaches that leverage the pre-trained capabilities of Flux to enhance text generation at inference time. AMO Sampler [13] improves text rendering accuracy by introducing a stochastic sampler along with a mask based on cross attention, but lacks explicit control over text positioning. TextCrafter [8] addresses the multi-text rendering task by separately denoising layout regions where text is generated and re-weighting attention maps to mitigate text blurring. But it often struggles to achieve seamless integration between text regions and the background, resulting in unnatural visual transitions. Furthermore, both methods still suffer from limited text accuracy and inference-time computational overhead.

2.2. Attention Control

Attention maps have been widely explored for controlling generation in diffusion models. Prompt-to-Prompt [12] reveals that cross-attention maps reflect spatial alignment between prompt and image, which can be exploited for prompt-based image editing by replacing or re-weighting these maps. Additional techniques compute loss signals from attention maps and apply latent updates to better align outputs with textual prompts [1, 3, 28]. Other approaches extend this idea to incorporate layout conditioning, enabling models to reflect both prompt semantics and spatial constraints [7, 39]. However, these methods rely solely on cross-attention mechanism, which limits their flexibility in capturing fine-grained spatial relationships. In addition, the latent update procedures introduce extra memory and computational overhead during inference.

More recently, MM-DiT-based models have adopted joint attention mechanisms, where text and image tokens are concatenated and jointly attended. Some studies apply spatial masks directly to joint attention maps to enforce layout constraints without latent updates. For instance, Regional-Prompting [4] enables compositional generation by performing both manipulated and unmanipulated attention evaluations, which doubles number of function evaluations (NFE) per denoising step. In contrast, DreamRenderer [43] replicates image tokens for each instance during attention, leading to substantial overhead within each step, instead of doubling NFE. Above all, these approaches mainly focus on generic objects while overlooking text, which is more difficult to generate due to strict requirements on glyph accuracy and character sequencing—especially when rendering large amounts of text.

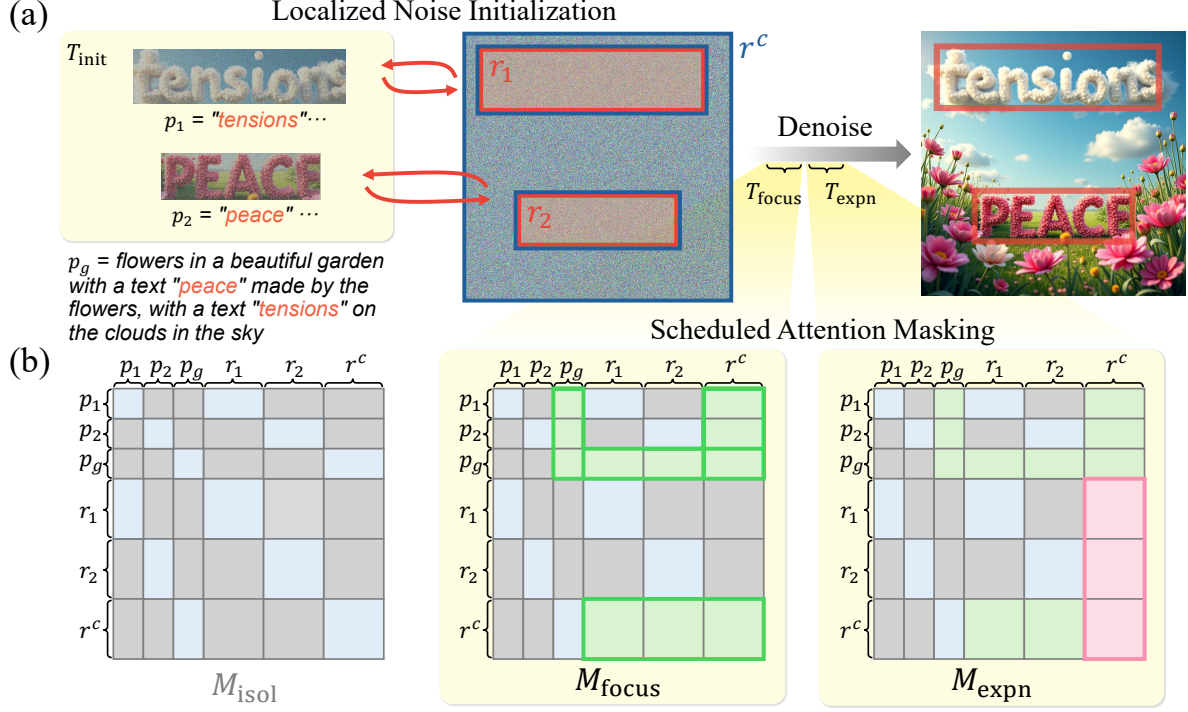


Figure 2. **Overview of DCText.** (a) Textual regions (r_1, r_2) are extracted from the initial noise and independently denoised with their textual prompts (p_1, p_2) for T_{init} steps. The refined patches are then blended back to form the localized initial noise. (b) It is then sequentially denoised using two attention masks, M_{focus} and M_{expn} . Both masks build on M_{isol} , which restricts attention to text and image tokens within each region (blue). M_{focus} introduces four attention areas (green) to allow controlled information flow between textual regions and the background, supporting accurate text rendering. M_{expn} further enables region-to-background attention (pink) to promote smooth transitions. In all three masks, colored areas denote allowed attention (1), while gray areas indicate masked attention (0).

3. Method

Our goal is to accurately and naturally generate texts from a global prompt, which may contain long or multiple sentences. To achieve this, we leverage bounding box conditions: given a set of regions requiring visual text segments (textual regions) and a global prompt, we extract the target texts embedded in the prompt and divide them to match the number of regions, generating each within its assigned region. Building on the attention mechanism of the Multi-Modal Diffusion Transformer, we control the information flow between textual and non-textual content (both across prompts and regions) using carefully designed attention masks. This approach enables region-centric text generation while ensuring smooth transitions in the background, keeping the overall image coherent with the global prompt. Our method, DCText, improves text accuracy by applying these attention masks at inference time, with minimal overhead compared to the base text-to-image model. It requires no training or fine-tuning and avoids heavy computations such as gradient calculations during inference [1, 28].

In the following sections, we first review the attention mechanism in MM-DiT (Sec. 3.1), then describe how this

attention is regulated by two novel attention masks and their design formulation (Sec. 3.2), next present the strategy for obtaining the initial noise (Sec. 3.3), and finally outline the overall DCText pipeline (Sec. 3.4).

3.1. Preliminary: Attention in MM-DiT

Recent T2I models [9, 15] employ MM-DiT blocks, which operate on a unified token sequence formed by concatenating text and image tokens. Each block computes attention over this combined sequence as follows:

$$\text{Attn}(Q, K, V) = AV, \quad A = \text{softmax} \left(\frac{QK^\top}{\sqrt{d}} \right), \quad (1)$$

where $Q = \text{concat}(Q_{\text{text}}, Q_{\text{img}})$, with Q_{text} and Q_{img} representing the queries derived from the text prompt tokens and image patch tokens, respectively; key (K) and value (V) are constructed in the same manner as Q .

During attention computation, it is possible to regulate the information flow between tokens by modifying or masking the attention map A . In particular, applying an attention mask M enables selective interaction by suppressing irrele-

vant connections while preserving meaningful ones:

$$A = \text{softmax} \left(\frac{QK^\top}{\sqrt{d}} + \log(M) \right). \quad (2)$$

Here, the binary values in M (1 for allowed connections, 0 for masked) are transformed via the log function into 0 and $-\infty$, respectively, to be added before the softmax operation.

3.2. Scheduled Attention Masking

We first decompose a global prompt, which contains multiple or lengthy target texts to be rendered, into a set of partial prompts (textual prompts) based on the number of textual regions n . For example, given a global prompt such as ‘*flowers in a beautiful garden with a text “peace” made by the flowers, with a text “tensions” on the clouds in the sky*’ and two regions, we construct textual prompts by separating *peace* and *tensions*, and assign each to its region.

These n textual prompts are encoded in the same manner as the global prompt, resulting in $\{p_i\}_{i=1}^n$. We extend the attention inputs Q , K , and V in Eq. (1) to incorporate both the textual prompts and the global prompt as follows:

$$Q_{\text{text}} = \text{concat}(\{Q_{p_i}\}_{i=1}^n, Q_{p_g}), \quad (3)$$

where Q_{p_i} and Q_{p_g} are queries from the i -th textual prompt and the global prompt, respectively. In parallel, we organize the image-side query Q_{img} not by extending it, but by decomposing it based on the textual regions. Specifically, image patches are divided into region-specific parts $\{r_i\}_{i=1}^n$ based on the given bounding boxes, and a background region $r^c = (\bigcup_{i=1}^n r_i)^c$, i.e. the complement of all regions:

$$Q_{\text{img}} = \text{concat}(\{Q_{r_i}\}_{i=1}^n, Q_{r^c}). \quad (4)$$

K and V are constructed analogously to Q .

We thus compute attention over the token sequence consisting of prompts $\{p_i\}_{i=1}^{n+1}$ and regions $\{r_i\}_{i=1}^{n+1}$, where $p_{n+1} = p_g$ and $r_{n+1} = r^c$. Note that the last prompt p_g serves as a global description that encompasses the textual prompts, while the last region r^c corresponds solely to the background region, excluding all textual regions.

In this setup, we propose two types of attention masks to guide the denoising process for accurate and coherent text generation. The text-focus attention mask M_{focus} biases the overall attention toward textual regions, enabling accurate text rendering at the correct regions while allowing the background to remain contextually natural. The context-expansion attention mask M_{expn} , on the other hand, further allows each textual region to attend to the background region, promoting smoother transitions and coherence at the boundaries between the region and the background.

To motivate the construction of these two masks, we first introduce the region-isolation attention mask M_{isol} , which enforces strict separation across all regions. While not used

Algorithm 1 DCText Pipeline

Input:

Prompts $\{p_i\}_{i=1}^{n+1}$ (with p_{n+1} : global prompt), Regions $\{r_i\}_{i=1}^{n+1}$ (with r_{n+1} : background), Denoising steps T , T_{init} , T_{focus} , T_{expn} , Blending weight α

Output:

Final image x_0

```

1: Make attention masks  $M_{\text{focus}}$ ,  $M_{\text{expn}}$ 
2: Sample  $z_T \sim \mathcal{N}(0, I)$  ▷ Localized Noise Initialization
3: for  $i = 1$  to  $n$  do
4:    $z^{(i)} \leftarrow \text{Extract}(z_T, r_i)$ 
5:   for  $t$  for  $T_{\text{init}}$  steps do
6:      $z^{(i)} \leftarrow \text{Denoise}(z^{(i)}, p_i)$ 
7:   end for
8:    $z_T \leftarrow \text{Reinsert}(z_T, r_i, z^{(i)}, \alpha)$ 
9: end for
10:  $z \leftarrow z_T$  ▷ Text-Focus Denoising
11: for  $t$  for  $T_{\text{focus}}$  steps do
12:    $z \leftarrow \text{DenoiseWithMask}(z, \{p_i\}_{i=1}^{n+1}, M_{\text{focus}})$ 
13: end for ▷ Context-Expansion Denoising
14: for  $t$  for  $T_{\text{expn}}$  steps do
15:    $z \leftarrow \text{DenoiseWithMask}(z, \{p_i\}_{i=1}^{n+1}, M_{\text{expn}})$ 
16: end for ▷ Global Denoising
17: for  $t$  for  $T - (T_{\text{init}} + T_{\text{focus}} + T_{\text{expn}})$  steps do
18:    $z \leftarrow \text{Denoise}(z, p_{n+1})$ 
19: end for
20: return  $\text{Decode}(z)$ 

```

in our method, M_{isol} serves as a conceptual foundation from which our proposed masks are derived. In the following, we detail the formulation of M_{isol} and then construct M_{focus} and M_{expn} by gradually relaxing the strict constraints imposed by M_{isol} . These masks are illustrated in Fig. 2b.

Region-Isolation Attention Mask. Our divide-and-conquer approach begins by partitioning the task, enabling each textual prompt to render its target text independently within its assigned region. This is enabled by constructing an isolated attention mask that implicitly regulates inter-region interactions, ensuring that each region focuses solely on its target text. Specifically, we enforce that only the text and image tokens associated with a particular region (i.e., $\{p_i, r_i\}$) can attend to one another, both across and within modalities. Let $m_{p_i} \in \{0, 1\}^{L_T}$ and $m_{r_i} \in \{0, 1\}^{L_I}$ be binary masks that activate only the token indices of the i -th textual prompt and its corresponding region, respectively. Here, L_T is the total number of text tokens across all $n+1$ prompts, and L_I is the number of image patch tokens (i.e.,



Figure 3. **Qualitative comparison on single sentence.** Prompts, including the sentence to be rendered (highlighted in red), are shown below each column. All comparisons are generated from the same initial noise.

$h \times w$). By concatenating m_{p_i} and m_{r_i} , we construct a joint mask $m_i \in \{0, 1\}^{L_T + L_I}$ that activates all text and image tokens associated with the i -th region, while masking out the rest. We then obtain the region-isolation attention mask M_{isol} by summing the outer products of these masks:

$$M_{\text{isol}} = \sum_{i=1}^{n+1} m_i \cdot m_i^\top \in \{0, 1\}^{(L_T + L_I) \times (L_T + L_I)}, \quad (5)$$

where \cdot denotes an outer product, resulting in a square mask.

However, while applying this mask allows each region to render its target text correctly, the resulting image fails to follow the global prompt. This occurs because M_{isol} eliminates all information flow between textual regions and the background, causing each region to be generated independently according to its own prompt. As a result, the final image may appear unnatural, as if multiple disjoint images were stitched together. Moreover, the background region, guided solely by the global prompt, may re-render text that is already rendered within the individual textual regions (left image in Fig. 6). In other words, this approach only divides the task but fails to conquer it.

Text-Focus Attention Mask. To address the limitations of M_{isol} , DCText expands the attendable regions in the mask (*i.e.* areas with value 1), allowing directional information flow between the textual regions, the background region, the textual prompts, and the global prompt.

For the background region, we allow it to attend to the textual regions so that the background can connect naturally to the text areas and avoid redundant text generation within the background. The subscript arrow $r^c \rightarrow \{r_i\}$ indicates the direction of attention from query to key:

$$M_{r^c \rightarrow \{r_i\}} = m_{r^c} \cdot \mathbf{1}_{L_I}^\top \in \{0, 1\}^{L_I \times L_I}. \quad (6)$$

We also allow the background region to be attended by the textual prompts, enabling each prompt to incorporate surrounding visual context. This helps the prompts generate more natural and contextually appropriate descriptions, leading to more accurate text rendering:

$$M_{\{p_i\} \rightarrow r^c} = \mathbf{1}_{L_T} \cdot m_{r^c}^\top \in \{0, 1\}^{L_T \times L_I}. \quad (7)$$

For the global prompt, we apply a similar strategy: enabling it to attend to the textual regions and receive attention

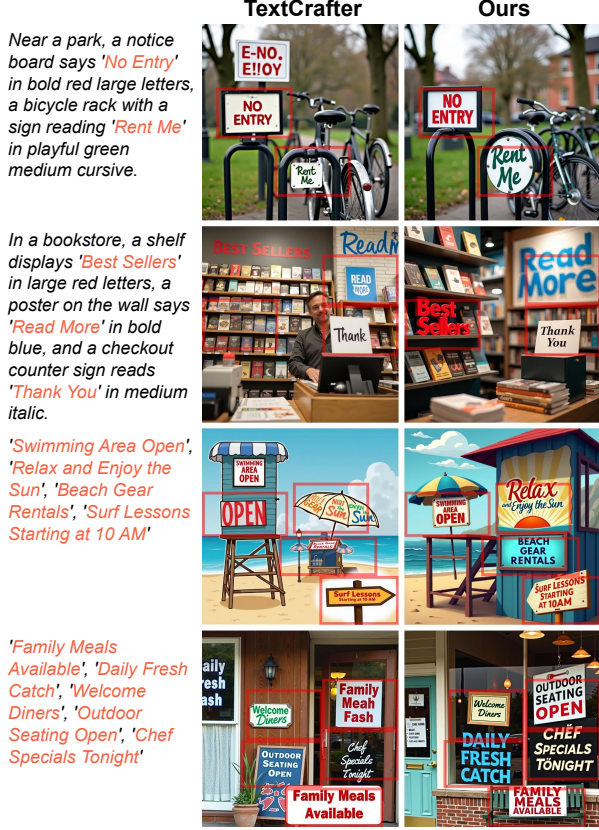


Figure 4. **Qualitative comparison on multiple sentences.** Comparison of generation results with varying numbers of sentences (2–5) in a single prompt. Sentences and corresponding regions are highlighted in red (only target texts are shown for the two prompts below; full prompts are in Appendix E.3). Our method consistently renders accurate text in the correct regions.

from the textual prompts. This promotes better coordination across the image and contributes to more natural and accurate text rendering (see Appendix B.1):

$$M_{p_g \rightarrow \{r_i\}} = m_{p_g} \cdot \mathbf{1}_{L_I}^\top \in \{0, 1\}^{L_I \times L_I}, \quad (8)$$

$$M_{\{p_i\} \rightarrow p_g} = \mathbf{1}_{L_T} \cdot m_{p_g}^\top \in \{0, 1\}^{L_T \times L_T}.$$

Finally, the text-focus attention mask M_{focus} is constructed by combining M_{isol} with the four additional partial masks defined above:

$$M_{\text{focus}} = M_{\text{isol}} \vee \begin{bmatrix} M_{\{p_i\} \rightarrow p_g} & M_{\{p_i\} \rightarrow r^c} \vee M_{p_g \rightarrow \{r_i\}} \\ 0 & M_{r^c \rightarrow \{r_i\}} \end{bmatrix}. \quad (9)$$

Context-Expansion Attention Mask. While M_{focus} enables accurate text generation within the textual regions and allows the background to naturally incorporate these regions, the textual regions themselves still attend solely to their own content. In other words, each region remains

blind to the background, potentially leading to an interior that looks visually isolated from its surroundings (see Appendix Fig. S7). To address this, we allow textual regions to attend to the background after a few denoising steps with M_{focus} , once the target texts have been reasonably placed. This enables bidirectional information flow between the regions and the background:

$$M_{\{r_i\} \rightarrow r^c} = \mathbf{1}_{L_I} \cdot m_{r^c}^\top \in \{0, 1\}^{L_I \times L_I}, \quad (10)$$

$$M_{\text{expn}} = M_{\text{focus}} \vee \begin{bmatrix} 0 & 0 \\ 0 & M_{\{r_i\} \rightarrow r^c} \end{bmatrix}.$$

3.3. Localized Noise Initialization

We observe that generating text over an entire region-sized image is often easier than placing the same text within that region in the context of a full-sized image. Motivated by this, we propose a initialization strategy (Fig. 2a) that performs light denoising on region-specific noise patches, allowing each region to receive early guidance before global denoising begins. We first sample initial noise for the full image, $z_T \sim \mathcal{N}(0, I)$, where $z_T \in \mathbb{R}^{c \times h \times w}$. From z_T , we extract a set of localized noise patches $\{z_{T_i} \in \mathbb{R}^{c \times h_i \times w_i}\}_{i=1}^n$, each corresponding to a textual region $\{r_i\}_{i=1}^n$. Each patch z_{T_i} is then independently denoised for a very small number of steps using its associated textual prompt, yielding a lightly refined latent $z_{T'_i}$, where $T' = T - T_{\text{init}}$. These refined patches are blended back into their original locations within z_T using a weighting factor α , resulting in the updated global latent $z_{T'}$. Specifically, for each region r_i :

$$z_{T'}[r_i] = \alpha \cdot z_{T_i} + (1 - \alpha) \cdot z_{T'_i}. \quad (11)$$

After this initialization for T_{init} steps, we proceed with the remaining T' denoising steps using the updated latent $z_{T'}$. This simple initialization approach improves region-text spatial alignment and text rendering accuracy while remaining computationally efficient, as the total region area $\sum_i h_i w_i$ is smaller than the full image area hw .

3.4. DCText Pipeline

DCText divides the denoising process into four sequential stages: (1) Localized Noise Initialization for T_{init} steps, (2) Text-Focus denoising using the attention mask M_{focus} for T_{focus} steps, (3) Context-Expansion denoising using the attention mask M_{expn} for T_{expn} steps, and (4) standard denoising without attention masking control, using only the global prompt for the remaining steps. The full pseudocode of the DCText pipeline is provided in Algorithm 1.

4. Experiments

4.1. Experiment Setting

Benchmark. We evaluate our method on four datasets: ChineseDrawText [21], DrawTextCreative [17], TMDBE-

Method	Acc.	NED	CLIP	Qual.	Aesth.	Steps	Latency
Flux	0.266	0.579	0.343	4.657	3.851	24	13.89
AMO	0.274	0.569	0.342	4.658	3.863	28	25.93
TC	0.329	0.722	0.350	4.704	3.911	30	36.89
Ours	0.387	0.751	0.349	4.737	3.904	24	16.60

Table 1. **Quantitative comparison on single sentence.** Results are averaged over three single-sentence datasets (ChineseDrawText [21], DrawTextCreative [17], TMDBEval500 [5]). Steps and latency indicate denoising steps and total generation time per image (seconds, measured on an L40 GPU).

<i>n</i>	Method	Acc.	NED	CLIP	Qual.	Aesth.	Latency
5	Flux	0.366	0.608	0.336	4.591	3.165	13.91
	AMO	0.432	0.660	0.335	4.652	3.218	26.02
	TC	0.685	0.859	0.349	4.659	3.506	40.53
	Ours	0.693	0.860	0.343	4.697	3.569	19.26
4	Flux	0.389	0.628	0.338	4.707	3.421	13.93
	AMO	0.488	0.690	0.337	4.709	3.518	25.97
	TC	0.693	0.867	0.352	4.665	3.488	39.60
	Ours	0.760	0.892	0.353	4.745	3.659	18.14
3	Flux	0.508	0.715	0.345	4.662	3.377	13.88
	AMO	0.575	0.750	0.343	4.689	3.489	25.99
	TC	0.722	0.880	0.351	4.659	3.571	39.01
	Ours	0.768	0.906	0.351	4.735	3.709	16.96
2	Flux	0.608	0.809	0.344	4.675	3.471	13.88
	AMO	0.642	0.826	0.341	4.654	3.584	25.91
	TC	0.758	0.919	0.346	4.697	3.616	38.22
	Ours	0.792	0.923	0.347	4.791	3.726	15.66

Table 2. **Quantitative comparison on multiple sentences.** Comparison results on the CVTG-Style [8] dataset across different numbers of sentences (*n*) to be rendered.

val500 [5], and CVTG-Style [8]. The first three datasets mainly contain single-sentence prompts, while CVTG-Style includes prompts with 2–5 rendering sentences. These datasets cover diverse text rendering scenarios, from artistic typography to real-world scenes and stylized text.

Metric. We evaluate text rendering accuracy using sentence-level accuracy (Acc.) and Normalized Edit Distance (NED) [32], with PP-OCRv4 [22] for single-sentence prompts and GPT-4o [14] for multi-sentence prompts to handle sentence-level recognition. Image quality is assessed using Q-Align [37] for Quality and Aesthetic Scores, and CLIP Score [25] for prompt–image alignment. Latency per image generation is measured for efficiency, and a user study is conducted to assess preference.

Baselines. We compare our method against tuning-free visual text generation methods based on Flux.1-dev [15]: Flux, the base model; AMO Sampler (AMO) [13], a sampler that adaptively corrects sampling trajectories using attention weights; TextCrafter (TC) [8], explicitly isolating

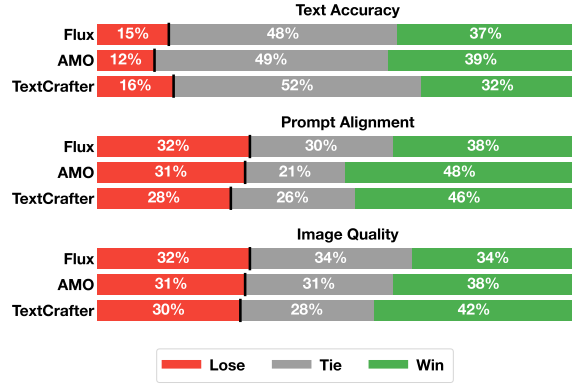


Figure 5. **Human Evaluation.** User preference on text accuracy, prompt–image alignment, and overall image quality. Green bars indicate cases where our method is preferred.

text regions for denoising and enhances attention for clearer rendering. All baselines use official implementations with default settings. Further comparisons with training-based methods and tuning-free methods based on Stable Diffusion 3.5 are provided in Appendix A.3 and C.2.

Implementation Details. We adopt Flux.1-dev [15] as our base model and generate all images at 1024×1024 resolution with 24 denoising steps. For each sentence in a prompt, we construct a textual prompt and region, using GPT-4o [14] for single-sentence cases and adopting CVTG-Style prompts while sharing regions from TextCrafter [8] for multi-sentence cases. We set $(T_{\text{init}}, T_{\text{focus}}, T_{\text{expn}})$ to (1,2,2) for single-sentence generation and (2,3,2) for multi-sentence generation; more details are in Appendix E.1.

4.2. Qualitative Results

Fig. 3 compares DCText with all tuning-free baselines on datasets containing single rendering sentences. In columns 1 and 4, baselines omit the sentence or produce only partial outputs, while our method generates the full text. In columns 2, 5, and 6, baselines generate incorrect or repeated text, whereas DCText produces the correct text as prompted. Notably, TextCrafter often produces text regions visually detached from the rest of the image (columns 3–5, *e.g.* with awkward white backgrounds), resulting in unnatural compositions. In contrast, DCText integrates text seamlessly into the scene, maintaining overall visual coherence.

Fig. 4 further compares our method with TextCrafter on multi-sentence generation. TextCrafter frequently fails to generate text within the designated areas or renders unintended text outside them (rows 1–3). As the number of regions increases (row 4), it often generates phrases in incorrect regions (*e.g.* “*OUTDOOR SEATING OPEN*”) or repeats the same phrase across different regions (*e.g.* “*Family*

Meals Available’’). This stems from its global attention operating over the entire image, which introduces cross-region interference even when denoising is applied independently per region. In contrast, with Localized Noise Initialization and the Text-Focus Attention Mask, our method enforces region-focused attention control, accurately rendering the text in each correct region while preventing cross-region interference. At the same time, background region remains text-free and blend naturally with the surrounding scene. Additional samples are provided in Appendix A.1.

4.3. Quantitative Results

Tab. 1 presents the results on three single-sentence datasets. In terms of text accuracy, DCText achieves 45% and 30% improvements over Flux in sentence-level accuracy and NED, respectively, outperforming all baselines. Notably, our method maintains high aesthetic and quality scores, showing that these improvements do not compromise generative priors of the base model. The high CLIP score further suggests that the model continues to follow the global prompt well, even when conditioned on decomposed multiple prompts. Remarkably, these gains are achieved with the fewest denoising steps and the lowest latency, requiring only about 20% additional latency compared to Flux. Latency is measured over the entire pipeline, including Localized Noise Initialization (1 step) and 23 denoising steps.

Tab. 2 compares DCText against all baselines on the multi-sentence dataset across varying numbers of regions. As in Tab. 1, our method consistently achieves the highest text accuracy without compromising image quality across all region counts. These results demonstrate the effectiveness of our divide-and-conquer strategy, which decomposes text by region and employs scheduled attention masking to ensure accurate and coherent text generation within the overall image context. Although latency increases slightly as the number of regions grows, it remains lower than all baselines except Flux, underscoring efficiency of DCText. More comprehensive results are available in Appendix A.2.

To further assess user preferences, we conduct a human evaluation across three datasets, assessing text accuracy, alignment between the image and the global prompt, and overall image quality, following the same protocol as Tab. 1. A total of 30 evaluators perform pairwise comparisons between DCText and each baseline over 1,323 image pairs (see Appendix E.2). The results, presented in Fig. 5, show that our method is consistently favored across all criteria, with particularly significant improvements in text accuracy.

4.4. Ablation Study

Tab. 3 and Fig. 6 present ablation results, evaluating each component of DCText. To assess the effectiveness of our proposed masks, we compare the combination of M_{focus} and M_{expn} against using only M_{isol} during the T_{focus} +

Method	Acc.	NED	CLIP	Qual.	Aesth.
M_{isol}	0.222	0.640	0.345	4.564	3.683
$M_{\text{focus}} + M_{\text{expn}}$	0.306	0.700	0.346	4.569	3.700
$T_{\text{init}} + M_{\text{focus}} + M_{\text{expn}}$	0.387	0.751	0.349	4.737	3.904

Table 3. **Ablation study on DCText components.** M_{isol} denotes denoising using only the isolation attention mask. $M_{\text{focus}} + M_{\text{expn}}$ uses our attention masks during two-stage denoising. $T_{\text{init}} + M_{\text{focus}} + M_{\text{expn}}$ further incorporates Localized Noise Initialization, forming our full pipeline.

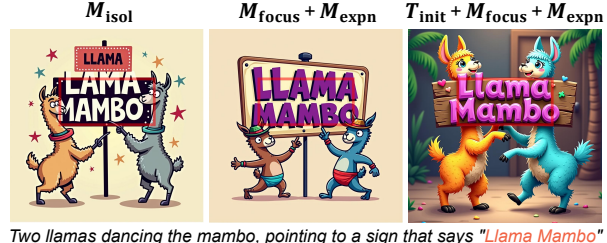


Figure 6. **Qualitative results of ablation study.** M_{isol} causes redundant text and harsh boundary, while $M_{\text{focus}} + M_{\text{expn}}$ yields accurate text and smooth transition. Localized Noise Initialization further enhances text-region alignment

T_{expn} steps. As shown in Fig. 6 (left) and the first row of Tab. 3, using M_{isol} results in redundant text rendering and lower text accuracy (Acc., NED). This is due to the textual region and background independently attending to separate prompts—a textual prompt and a global prompt. In addition, the restricted information flow enforced by M_{isol} creates a hard boundary around the region, preventing smooth transitions between the textual region and the background. In contrast, our two-stage masks ($M_{\text{focus}} + M_{\text{expn}}$) first focus attention on the textual region to prevent redundancy, and then gradually expand it to the background, enabling seamless transitions. This improves both text accuracy and overall image quality by achieving precise attention control between region and background. Finally, denoising from an latent obtained via Localized Noise Initialization (*i.e.* full DCText pipeline) provides region-specific guidance, achieving tighter alignment between rendered text and its region (right image in Fig. 6) and further boosting text accuracy (last row in Tab. 3). The sensitivity analysis of each component can be found in Appendix B.2–B.4.

5. Conclusion

We present DCText, a training-free method that adopts a divide-and-conquer strategy for accurate and coherent visual text generation. By decomposing target texts and guiding generation with scheduled attention masking, DCText improves text accuracy with the lowest latency among all compared methods, without degrading image quality.

Acknowledgement This work was supported by the National Research Foundation of Korea (NRF) grant funded by the Korea government (MSIT) [No. 2022R1A3B1077720; 2022R1A5A7083908], Institute of Information & Communications Technology Planning & Evaluation (IITP) grant funded by the Korea government (MSIT) [RS-2022-II220959; No.RS-2021-II211343, Artificial Intelligence Graduate School Program (Seoul National University)], the BK21 FOUR program of the Education and Research Program for Future ICT Pioneers, Seoul National University in 2025.

References

- [1] Aishwarya Agarwal, Srikrishna Karanam, KJ Joseph, Apoorv Saxena, Koustava Goswami, and Balaji Vasan Srinivasan. A-star: Test-time attention segregation and retention for text-to-image synthesis. In *Proceedings of the IEEE/CVF International Conference on Computer Vision*, pages 2283–2293, 2023. [2](#) [3](#)
- [2] James Betker, Gabriel Goh, Li Jing, Tim Brooks, Jianfeng Wang, Linjie Li, Long Ouyang, Juntang Zhuang, Joyce Lee, Yufei Guo, et al. Improving image generation with better captions. *Computer Science*. <https://cdn.openai.com/papers/dall-e-3.pdf>, 2(3):8, 2023. [15](#)
- [3] Hila Chefer, Yuval Alaluf, Yael Vinker, Lior Wolf, and Daniel Cohen-Or. Attend-and-excite: Attention-based semantic guidance for text-to-image diffusion models. *ACM transactions on Graphics (TOG)*, 42(4):1–10, 2023. [2](#)
- [4] Anthony Chen, Jianjin Xu, Wenzhao Zheng, Gaole Dai, Yida Wang, Renrui Zhang, Haofan Wang, and Shanghang Zhang. Training-free regional prompting for diffusion transformers. *arXiv preprint arXiv:2411.02395*, 2024. [2](#) [11](#) [21](#)
- [5] Jingye Chen, Yupan Huang, Tengchao Lv, Lei Cui, Qifeng Chen, and Furu Wei. Textdiffuser: Diffusion models as text painters. *Advances in Neural Information Processing Systems*, 36:9353–9387, 2023. [1](#) [2](#) [7](#) [11](#) [12](#) [15](#)
- [6] Jingye Chen, Yupan Huang, Tengchao Lv, Lei Cui, Qifeng Chen, and Furu Wei. Textdiffuser-2: Unleashing the power of language models for text rendering. In *European Conference on Computer Vision*, pages 386–402. Springer, 2024. [2](#) [11](#)
- [7] Omer Dahary, Or Patashnik, Kfir Aberman, and Daniel Cohen-Or. Be yourself: Bounded attention for multi-subject text-to-image generation. In *European Conference on Computer Vision*, pages 432–448. Springer, 2024. [2](#)
- [8] Nikai Du, Zhennan Chen, Zhizhou Chen, Shan Gao, Xi Chen, Zhengkai Jiang, Jian Yang, and Ying Tai. Textcrafter: Accurately rendering multiple texts in complex visual scenes. *arXiv preprint arXiv:2503.23461*, 2025. [1](#) [2](#) [7](#) [12](#) [14](#) [15](#)
- [9] Patrick Esser, Sumith Kulal, Andreas Blattmann, Rahim Entezari, Jonas Müller, Harry Saini, Yam Levi, Dominik Lorenz, Axel Sauer, Frederic Boesel, et al. Scaling rectified flow transformers for high-resolution image synthesis. In *Forty-first international conference on machine learning*, 2024. [3](#)
- [10] Patrick Esser, Sumith Kulal, Andreas Blattmann, Rahim Entezari, Jonas Müller, Harry Saini, Yam Levi, Dominik Lorenz, Axel Sauer, Frederic Boesel, et al. Scaling rectified flow transformers for high-resolution image synthesis. In *Forty-first International Conference on Machine Learning*, 2024. [1](#) [14](#) [15](#)
- [11] Dhruba Ghosh, Hannaneh Hajishirzi, and Ludwig Schmidt. Geneval: An object-focused framework for evaluating text-to-image alignment. *Advances in Neural Information Processing Systems*, 36:52132–52152, 2023. [13](#)
- [12] Amir Hertz, Ron Mokady, Jay Tenenbaum, Kfir Aberman, Yael Pritch, and Daniel Cohen-Or. Prompt-to-prompt image editing with cross attention control. *arXiv preprint arXiv:2208.01626*, 2022. [2](#)
- [13] Xixi Hu, Keyang Xu, Bo Liu, Qiang Liu, and Hongliang Fei. Amo sampler: Enhancing text rendering with overshooting, 2025. [1](#) [2](#) [7](#) [14](#) [15](#)
- [14] Aaron Hurst, Adam Lerer, Adam P Goucher, Adam Perelman, Aditya Ramesh, Aidan Clark, AJ Ostrow, Akila Welihinda, Alan Hayes, Alec Radford, et al. Gpt-4o system card. *arXiv preprint arXiv:2410.21276*, 2024. [7](#) [14](#) [15](#)
- [15] Black Forest Labs. Flux.1-dev. <https://huggingface.co/black-forest-labs/FLUX.1-dev>, 2024. [1](#) [3](#) [7](#) [15](#)
- [16] Jie Liu, Gongye Liu, Jiajun Liang, Yangguang Li, Jiaheng Liu, Xintao Wang, Pengfei Wan, Di Zhang, and Wanli Ouyang. Flow-grpo: Training flow matching models via online rl. *arXiv preprint arXiv:2505.05470*, 2025. [15](#)
- [17] Rosanne Liu, Dan Garrette, Chitwan Saharia, William Chan, Adam Roberts, Sharan Narang, Irina Blok, RJ Mical, Mohammad Norouzi, and Noah Constant. Character-aware models improve visual text rendering. *arXiv preprint arXiv:2212.10562*, 2022. [1](#) [2](#) [6](#) [7](#) [12](#) [15](#)
- [18] Zeyu Liu, Weicong Liang, Zhanhao Liang, Chong Luo, Ji Li, Gao Huang, and Yuhui Yuan. Glyph-byt5: A customized text encoder for accurate visual text rendering. In *European Conference on Computer Vision*, pages 361–377. Springer, 2024. [1](#)
- [19] Zeyu Liu, Weicong Liang, Yiming Zhao, Bohan Chen, Lin Liang, Lijuan Wang, Ji Li, and Yuhui Yuan. Glyph-byt5-v2: A strong aesthetic baseline for accurate multilingual visual text rendering. *arXiv preprint arXiv:2406.10208*, 2024. [2](#)
- [20] Runnan Lu, Yuxuan Zhang, Jiaming Liu, Haofan Wang, and Yiren Song. Easytext: Controllable diffusion transformer for multilingual text rendering. *arXiv preprint arXiv:2505.24417*, 2025. [11](#)
- [21] Jian Ma, Mingjun Zhao, Chen Chen, Ruichen Wang, Di Niu, Haonan Lu, and Xiaodong Lin. Glyphdraw: Seamlessly rendering text with intricate spatial structures in text-to-image generation. *arXiv preprint arXiv:2303.17870*, 2023. [2](#) [6](#) [7](#) [12](#) [15](#)
- [22] PaddlePaddle. Paddleocr. https://github.com/PaddlePaddle/PaddleOCR/blob/release/2.7/doc/doc_ch/PP-OCRv4_introduction.md, 2023. [7](#)
- [23] Dustin Podell, Zion English, Kyle Lacey, Andreas Blattmann, Tim Dockhorn, Jonas Müller, Joe Penna,

and Robin Rombach. Sdxl: Improving latent diffusion models for high-resolution image synthesis. *arXiv preprint arXiv:2307.01952*, 2023. 15

[24] Dustin Podell, Zion English, Kyle Lacey, Andreas Blattmann, Tim Dockhorn, Jonas Müller, Joe Penna, and Robin Rombach. Sdxl: Improving latent diffusion models for high-resolution image synthesis. In *The Twelfth International Conference on Learning Representations*, 2024. 1

[25] Alec Radford, Jong Wook Kim, Chris Hallacy, Aditya Ramesh, Gabriel Goh, Sandhini Agarwal, Girish Sastry, Amanda Askell, Pamela Mishkin, Jack Clark, et al. Learning transferable visual models from natural language supervision. In *International conference on machine learning*, pages 8748–8763. PMLR, 2021. 7

[26] Colin Raffel, Noam Shazeer, Adam Roberts, Katherine Lee, Sharan Narang, Michael Matena, Yanqi Zhou, Wei Li, and Peter J Liu. Exploring the limits of transfer learning with a unified text-to-text transformer. *Journal of machine learning research*, 21(140):1–67, 2020. 1

[27] Aditya Ramesh, Prafulla Dhariwal, Alex Nichol, Casey Chu, and Mark Chen. Hierarchical text-conditional image generation with clip latents. *arXiv preprint arXiv:2204.06125*, 1 (2):3, 2022. 15

[28] Royi Rassin, Eran Hirsch, Daniel Glickman, Shauli Ravfogel, Yoav Goldberg, and Gal Chechik. Linguistic binding in diffusion models: Enhancing attribute correspondence through attention map alignment. *Advances in Neural Information Processing Systems*, 36:3536–3559, 2023. 2, 3

[29] Robin Rombach, Andreas Blattmann, Dominik Lorenz, Patrick Esser, and Björn Ommer. High-resolution image synthesis with latent diffusion models. In *Proceedings of the IEEE/CVF conference on computer vision and pattern recognition*, pages 10684–10695, 2022. 1

[30] Robin Rombach, Andreas Blattmann, Dominik Lorenz, Patrick Esser, and Björn Ommer. High-resolution image synthesis with latent diffusion models. In *Proceedings of the IEEE/CVF conference on computer vision and pattern recognition*, pages 10684–10695, 2022. 2, 15

[31] Chitwan Saharia, William Chan, Saurabh Saxena, Lala Li, Jay Whang, Emily L Denton, Kamyar Ghasemipour, Raphael Gontijo Lopes, Burcu Karagol Ayan, Tim Salimans, et al. Photorealistic text-to-image diffusion models with deep language understanding. *Advances in neural information processing systems*, 35:36479–36494, 2022. 1

[32] Yuxiang Tuo, Wangmeng Xiang, Jun-Yan He, Yifeng Geng, and Xuansong Xie. Anytext: Multilingual visual text generation and editing. *arXiv preprint arXiv:2311.03054*, 2023. 1, 2, 7, 11

[33] Tong Wang, Xiaochao Qu, and Ting Liu. Textmastero: Mastering high-quality scene text editing in diverse languages and styles. *arXiv preprint arXiv:2408.10623*, 2024.

[34] Yibin Wang, Weizhong Zhang, Changhai Zhou, and Cheng Jin. High fidelity scene text synthesis. *arXiv preprint arXiv:2405.14701*, 2024. 2

[35] Yibin Wang, Weizhong Zhang, Honghui Xu, and Cheng Jin. Dreamtext: High fidelity scene text synthesis. In *Proceedings of the Computer Vision and Pattern Recognition Conference*, pages 28555–28563, 2025. 2

[36] Zhendong Wang, Jianmin Bao, Shuyang Gu, Dong Chen, Wengang Zhou, and Houqiang Li. Designndiffusion: High-quality text-to-design image generation with diffusion models. In *Proceedings of the Computer Vision and Pattern Recognition Conference*, pages 20906–20915, 2025. 2

[37] Haoning Wu, Zicheng Zhang, Weixia Zhang, Chaofeng Chen, Liang Liao, Chunyi Li, Yixuan Gao, Annan Wang, Erli Zhang, Wenxiu Sun, et al. Q-align: Teaching lmms for visual scoring via discrete text-defined levels. *arXiv preprint arXiv:2312.17090*, 2023. 7

[38] Enze Xie, Junsong Chen, Yuyang Zhao, Jincheng Yu, Ligeng Zhu, Chengyue Wu, Yujun Lin, Zhekai Zhang, Muyang Li, Junyu Chen, et al. Sana 1.5: Efficient scaling of training-time and inference-time compute in linear diffusion transformer. *arXiv preprint arXiv:2501.18427*, 2025. 15

[39] Jinheng Xie, Yuexiang Li, Yawen Huang, Haozhe Liu, Wentian Zhang, Yefeng Zheng, and Mike Zheng Shou. Boxdiff: Text-to-image synthesis with training-free box-constrained diffusion. In *Proceedings of the IEEE/CVF International Conference on Computer Vision*, pages 7452–7461, 2023. 2

[40] Yukang Yang, Dongnan Gui, Yuhui Yuan, Weicong Liang, Haisong Ding, Han Hu, and Kai Chen. Glyphcontrol: Glyph conditional control for visual text generation. *Advances in Neural Information Processing Systems*, 36:44050–44066, 2023. 1, 2, 11

[41] Weichao Zeng, Yan Shu, Zhenhang Li, Dongbao Yang, and Yu Zhou. Textctrl: Diffusion-based scene text editing with prior guidance control. *Advances in Neural Information Processing Systems*, 37:138569–138594, 2024. 2

[42] Yiming Zhao and Zhouhui Lian. Udifftext: A unified framework for high-quality text synthesis in arbitrary images via character-aware diffusion models. In *European conference on computer vision*, pages 217–233. Springer, 2024. 2

[43] Deweい Zhou, Mingwei Li, Zongxin Yang, and Yi Yang. Dreamrenderer: Taming multi-instance attribute control in large-scale text-to-image models. *arXiv preprint arXiv:2503.12885*, 2025. 2

Appendix

A. Additional Results

A.1. Qualitative Samples

Fig. S1 and Fig. S2 present additional qualitative samples generated by DCText. As shown in the results, our method consistently produces accurate text and high-quality images across a wide range of themes, including illustrations, real scenes, posters, artistic styles, and animations. Notably, these results are achieved without any additional training, relying solely on scheduled attention masking at inference time. In particular, Fig. S2 demonstrates that the textual regions faithfully reflect the target sentences, even when multiple texts need to be rendered. At the same time, the overall image remains thematically aligned with the global prompt. This is enabled by DCText’s attention masks (M_{focus} , M_{expn}), which effectively regulate the information flow between the target regions and the background.

A.2. Quantitative Results

Tab. S1 provides a comprehensive comparison across all datasets and baselines. To support broader evaluation, we additionally report baseline results obtained using the same number of denoising steps as our method, indicated by \dagger . For text accuracy metrics (Acc. and NED), DCText consistently outperforms all baselines across all datasets. This underscores the effectiveness of our divide-and-conquer strategy, which generates text segments rather than entire sentences at once, resulting in more reliable text generation. In terms of overall image quality (Qual. and Aesth.), our method also achieves high scores on most datasets, indicating that improvements in text accuracy do not come at the expense of image quality. In addition, when baselines are evaluated under the same reduced number of denoising steps, their performance typically declines across most metrics. Although this setting reduces inference latency, our method still maintains the lowest latency, with strong performance.

A.3. Comparison with Training-based Methods

In the main paper, we compare DCText with other approaches that, like ours, leverage a pre-trained text-to-image model without additional training. We further compare our method against training-based approaches, including AnyText [32], GlyphControl [40], TextDiffuser2 [6], and EasyText [20]. Tab. S2 presents a quantitative comparison on the single-sentence datasets. In terms of text accuracy (Acc. and NED), training-based baselines—trained on large-scale text-centric datasets (AnyWord-3M [32], LAION-Glyph [40], MARIO-10M [5], and EasyText-1M [20]) with glyph-level conditioning—generally achieve higher scores. However, this comes at the cost of overall image quality. As

reflected by their low aesthetic scores (Aesth.)—and as visually confirmed in Fig. S3—training-based methods lack stylistic diversity and fail to produce artistic text. For instance, in columns 3 and 4, where the prompts specify rendering text with fur and vines, these methods generate plain, generic text instead of following the intended styles. In the more challenging multi-sentence setting, training-based approaches also struggle. As shown in Tab. S3, their text accuracy degrades significantly as the number of sentences (n) increases. In contrast, DCText maintains consistent performance and outperforms all baselines across different sentence counts.

A.4. Comparison to Regional-Prompting

To highlight DCText’s performance in visual text generation, we compare it with Regional-Prompting [4], a method that relies solely on the Region-Isolation Attention Mask (M_{isol}) for inference-time attention control. As discussed in Sec. 3.2, the exclusive use of M_{isol} often results in redundant text rendering and unnatural regional artifacts (see Fig. 6, left). Regional-Prompting addresses this by replacing the global prompt with a background-only prompt, removing all content information, and additionally performs a separate denoising process with the original global prompt, spatially blending the two resulting latents. However, this approach not only doubles the number of function evaluations (NFEs), but also remains less effective for visual text generation. As shown in Fig. S4, Regional-Prompting often produces illegible or semantically meaningless text. This occurs because the fine-detailed visual features required for faithful text rendering are diluted during latent blending. In contrast, DCText generates text that is both accurate and natural, while also requiring only 15.66 seconds per image generation compared to 27.79 seconds for Regional-Prompting. This demonstrates that our two novel masks—Text-Focus Attention Mask (M_{focus}) and Context-Expansion Attention Mask (M_{expn})—enable effective and efficient attention control for visual text generation.

B. Additional Ablation Studies

B.1. Text-Focus Attention Mask Design

To construct M_{focus} , we take the union of four partial masks ($M_{r^c \rightarrow \{r_i\}}$, $M_{\{p_i\} \rightarrow r^c}$, $M_{p_g \rightarrow \{r_i\}}$, $M_{\{p_i\} \rightarrow p_g}$), each of which enables a specific directional attention flow. To evaluate the contribution of each component, we conduct an ablation study by selectively excluding individual partial masks. The results are shown in Fig. S5 and Tab. S4. When the attention flow from the background region to the textual regions is disabled (*i.e.* w/o $M_{r^c \rightarrow \{r_i\}}$), duplicated text tends to appear in the background, and the transition between background and target regions becomes unnatural. The awkward bright areas of the first row in Fig. S5 illus-

Dataset	n	Method	Acc.	NED	CLIP	Qual.	Aesth.	Steps	Latency (sec.)
CreativeDrawText	1	Flux	0.257	0.544	0.339	4.695	3.718	24	13.89
		AMO	0.261	0.559	0.339	4.691	3.693	28	25.93
		AMO \dagger	0.193	0.524	0.338	4.697	3.707	24	21.71
		TextCrafter	0.330	0.764	0.346	4.726	3.767	30	36.89
		TextCrafter \dagger	0.330	0.750	0.346	4.727	3.722	24	28.61
		DCText (Ours)	0.427	0.809	0.345	4.775	3.761	24	16.60
DrawTextCreative	1	Flux	0.223	0.525	0.351	4.657	3.774	24	13.81
		AMO	0.234	0.499	0.351	4.670	3.831	28	25.99
		AMO \dagger	0.234	0.516	0.350	4.624	3.755	24	21.76
		TextCrafter	0.286	0.645	0.351	4.698	3.848	30	36.92
		TextCrafter \dagger	0.286	0.664	0.353	4.691	3.855	24	28.61
		DCText (Ours)	0.337	0.675	0.350	4.765	3.934	24	16.61
TMDBEval500	1	Flux	0.318	0.667	0.340	4.618	4.061	24	13.88
		AMO	0.326	0.648	0.336	4.614	4.064	28	25.89
		AMO \dagger	0.340	0.665	0.338	4.607	4.041	24	21.74
		TextCrafter	0.372	0.758	0.352	4.687	4.119	30	36.91
		TextCrafter \dagger	0.358	0.744	0.351	4.661	4.074	24	28.63
		DCText (Ours)	0.396	0.768	0.351	4.670	4.018	24	16.56
CVTG-Style	2	Flux	0.608	0.809	0.344	4.675	3.471	24	13.88
		AMO	0.642	0.826	0.341	4.654	3.584	28	25.91
		AMO \dagger	0.622	0.820	0.341	4.664	3.580	24	21.98
		TextCrafter	0.758	0.919	0.346	4.697	3.616	30	38.22
		TextCrafter \dagger	0.745	0.923	0.348	4.688	3.584	24	28.97
		DCText (Ours)	0.792	0.923	0.347	4.791	3.726	24	15.66
CVTG-Style	3	Flux	0.508	0.715	0.345	4.662	3.377	24	13.88
		AMO	0.575	0.750	0.343	4.689	3.489	28	25.99
		AMO \dagger	0.540	0.741	0.342	4.679	3.480	24	21.86
		TextCrafter	0.722	0.880	0.351	4.659	3.571	30	39.01
		TextCrafter \dagger	0.710	0.882	0.350	4.670	3.595	24	29.47
		DCText (Ours)	0.768	0.906	0.351	4.735	3.709	24	16.96
CVTG-Style	4	Flux	0.389	0.628	0.338	4.707	3.421	24	13.93
		AMO	0.488	0.690	0.337	4.709	3.518	28	25.97
		AMO \dagger	0.469	0.689	0.337	4.709	3.515	24	21.97
		TextCrafter	0.693	0.867	0.352	4.665	3.488	30	39.60
		TextCrafter \dagger	0.722	0.877	0.354	4.697	3.530	24	30.07
		DCText (Ours)	0.760	0.892	0.353	4.745	3.659	24	18.14
CVTG-Style	5	Flux	0.366	0.608	0.336	4.591	3.165	24	13.91
		AMO	0.432	0.660	0.335	4.652	3.218	28	26.02
		AMO \dagger	0.402	0.636	0.336	4.618	3.190	24	21.94
		TextCrafter	0.685	0.859	0.349	4.659	3.506	30	40.53
		TextCrafter \dagger	0.661	0.848	0.343	4.562	3.396	24	30.78
		DCText (Ours)	0.693	0.860	0.343	4.697	3.569	24	19.26
Average	-	Flux	0.381	0.642	0.342	4.658	3.570	24	13.88
		AMO	0.423	0.662	0.340	4.668	3.628	28	25.96
		AMO \dagger	0.400	0.656	0.340	4.657	3.610	24	21.84
		TextCrafter	0.549	0.813	0.350	4.684	3.702	30	38.30
		TextCrafter \dagger	0.545	0.813	0.349	4.671	3.679	24	29.31
		DCText (Ours)	0.596	0.833	0.349	4.740	3.768	24	17.11

Table S1. **Full quantitative comparison.** Comparison results with baselines on four datasets: ChineseDrawText [21], DrawTextCreative [17], TMDBEval500 [5], and CVTG-Style [8]. \dagger indicates methods that use the same number of denoising steps as DCText.

Method	Acc.	NED	Qual.	Aesth.
AnyText	0.096	0.442	4.128	2.990
GlyphControl	0.630	0.901	3.935	2.884
TextDiffuser2	0.552	0.860	3.463	2.488
EasyText	0.159	0.484	4.380	3.361
DCText (Ours)	0.387	0.751	4.737	3.904

Table S2. **Quantitative comparison between training-based baselines.** Results are averaged over three single-sentence datasets (ChineseDrawText, DrawTextCreative, TMDBEval500).

trate this issue. Disabling the attention flow from textual prompts to the background region (w/o $M_{\{p_i\} \rightarrow r^c}$) often causes incorrect text to be generated, significantly lowering text accuracy. When the attention from the global prompt to the textual regions is blocked (w/o $M_{p_g \rightarrow \{r_i\}}$), irrelevant text tends to appear. On the other hand, removing the attention from textual prompts to the global prompt (w/o $M_{\{p_i\} \rightarrow p_g}$) produces text that is less stylistically aligned with the overall image. Overall, incorporating all four directional attention flows results in the highest text accuracy and consistently high image quality.

B.2. Text-Focus Denoising Steps

Fig. S6 and Tab. S5 present the results of an ablation study on varying the number of denoising steps T_{focus} during which the text-focus attention mask M_{focus} is applied, while keeping T_{init} and T_{expn} fixed. As shown in the figure, when $T_{\text{focus}} = 0$, that is, when M_{focus} is not applied, the model fails to focus on the designated region, often producing region-irrelevant or entirely missing text. As T_{focus} increases, alignment between the generated text and the target region improves. However, excessive values of T_{focus} prevent regions from attending to the background for extended periods, leading to more noticeable boundaries between regions and their surroundings, and, as shown in the table, even causing a decline in text accuracy.

B.3. Context-Expansion Denoising Steps

To assess the contribution of the context-expansion attention mask M_{expn} , we conduct an ablation study varying the number of denoising steps allocated to the text-focus phase (T_{focus}) and the context-expansion phase (T_{expn}), keeping the total number of $T_{\text{focus}} + T_{\text{expn}}$ steps fixed (*i.e.* gradually substituting M_{focus} with M_{expn}). Fig. S7 and Tab. S6 show qualitative and quantitative results under different allocations of these steps. When $T_{\text{expn}} = 0$ (leftmost column), the target text is accurately aligned within the designated region, but the lack of attention to surrounding context results in sharp and unnatural boundaries between the region and background. As more steps are allocated to context-expansion, this boundary effect is gradually alleviated, leading to more visually natural results. However, when T_{expn}

n	Method	Acc.	NED	Qual.	Aesth.
5	AnyText	0.065	0.275	4.160	2.647
	GlyphControl	0.490	0.722	3.679	2.369
	TextDiffuser2	0.028	0.241	3.847	2.565
	EasyText	0.405	0.744	4.049	2.502
	DCText (Ours)	0.693	0.860	4.697	3.569
4	AnyText	0.052	0.269	4.324	2.815
	GlyphControl	0.507	0.729	3.867	2.512
	TextDiffuser2	0.081	0.321	3.869	2.493
	EasyText	0.454	0.759	4.235	2.717
	DCText (Ours)	0.760	0.892	4.745	3.659
3	AnyText	0.054	0.261	4.281	2.781
	GlyphControl	0.610	0.795	3.853	2.521
	TextDiffuser2	0.252	0.508	3.785	2.439
	EasyText	0.433	0.762	4.266	2.747
	DCText (Ours)	0.768	0.906	4.735	3.709
2	AnyText	0.052	0.275	4.386	2.857
	GlyphControl	0.692	0.862	4.009	2.624
	TextDiffuser2	0.528	0.729	3.755	2.438
	EasyText	0.460	0.791	4.363	2.870
	DCText (Ours)	0.792	0.923	4.791	3.726

Table S3. **Quantitative comparison between training-based baselines.** Comparison results on the CVTG-Style dataset across different numbers of sentences (n).

becomes too dominant, information within the region starts to leak outward, leading to text generation that is no longer confined to the intended region (similar to the failure cases shown in the leftmost examples of Fig. S6). These results highlight the importance of a balanced sequential application of T_{focus} and T_{expn} —where T_{focus} helps localize the text within the target region, and T_{expn} promotes natural integration into the full image. Tab. S6 further supports this finding: both overly strong text-focus attention (first row) and excessive context-expansion (last row) lead to performance drops, while a balanced allocation yields the balanced high performance across all metrics.

B.4. Localized Noise Initialization Steps

As shown in Fig. S8 and Tab. S7, increasing T_{init} improves text alignment within textual regions and enhances text accuracy. However, since this approach creates an initial latent with uneven noise levels between region and background, we observe that setting $T_{\text{init}} > 2$ leads to image collapse under our experimental setup with 24 denoising steps.

C. Broader Applications of DCText

C.1. General Object

While DCText is primarily designed to address the challenging task of rendering long or multiple texts, its core strategy generalizes effectively to broader visual generation tasks. To evaluate this generality, we apply DCText to the GenEval [11] benchmark, which focuses on the compo-

Mask	Acc.	NED	CLIP	Qual.	Aesth.
w/o $M_{r^c \rightarrow \{r_i\}}$	0.275	0.683	0.347	4.721	3.878
w/o $M_{\{p_i\} \rightarrow r^c}$	0.266	0.666	0.345	4.735	3.885
w/o $M_{p_g \rightarrow \{r_i\}}$	0.330	0.721	0.350	4.733	3.890
w/o $M_{\{p_i\} \rightarrow p_g}$	0.347	0.732	0.349	4.746	3.921
M_{focus}	0.387	0.751	0.349	4.737	3.904

Table S4. **Ablation study for M_{focus} design.** Each row reports the result when one of the partial masks (defined in Sec. 3.2) is removed, evaluated on the single-sentence datasets.

T_{focus}	Acc.	NED	CLIP	Qual.	Aesth.
0	0.273	0.626	0.344	4.739	3.888
1	0.316	0.701	0.348	4.740	3.905
2	0.387	0.751	0.349	4.737	3.904
3	0.372	0.757	0.350	4.728	3.894
4	0.337	0.746	0.349	4.717	3.875

Table S5. **Ablation study for T_{focus} steps.** Quantitative results for different values of T_{focus} , evaluated on the single-sentence datasets.

sitional generation of general objects. In this experiment, we follow the original DCText pipeline as-is, but modify the GPT-4o [14] instructions for constructing textual prompts and regions. For textual prompts, we extract the target object from the global prompt and generate an object-centric prompt that includes a description aligned with the global context. For textual regions, we revise the original text-based instructions into object-based ones. We use the same denoising schedule as in the text generation setup: $(T_{\text{init}}, T_{\text{focus}}, T_{\text{expn}}) = (1, 2, 2)$ for single-object generation and $(2, 3, 2)$ for multi-object generation.

Fig. S9 shows qualitative results, and Tab. S8 summarizes quantitative comparisons. For evaluation, we generate four samples per prompt across all 553 prompts in the benchmark. As shown, DCText significantly outperforms the base model Flux, improving the overall GenEval score from 0.66 to 0.78. These results demonstrate the strong generalization capability of DCText beyond text rendering.

C.2. Stable Diffusion 3.5

We further evaluate the performance of DCText on another Multi-Modal Diffusion Transformer model, Stable Diffusion 3.5 Large (SD3.5-L) [10]. Following the same experimental setup as in the main paper, we also compare DCText against the same three baselines: SD3.5-L (the base model), AMO Sampler [13], and TextCrafter [8]. For fair comparison, we use a fixed number of 28 denoising steps across all methods, while keeping all other configurations at their respective defaults. As the AMO Sampler does not provide an official implementation for SD3.5, we re-implement it ourselves.

$T_{\text{expn}}(T_{\text{focus}})$	Acc.	NED	CLIP	Qual.	Aesth.
0 (4)	0.289	0.681	0.347	4.716	3.829
1 (3)	0.339	0.723	0.349	4.739	3.895
2 (2)	0.387	0.751	0.349	4.737	3.904
3 (1)	0.340	0.750	0.350	4.731	3.905
4 (0)	0.336	0.746	0.349	4.725	3.889

Table S6. **Ablation study for T_{expn} steps.** Quantitative results under different allocations of T_{expn} and T_{focus} (values in parentheses). As T_{expn} increases, T_{focus} is reduced accordingly, evaluated on the single-sentence datasets.

T_{init}	Acc.	NED	CLIP	Qual.	Aesth.
0	0.600	0.798	0.347	4.640	3.538
1	0.717	0.878	0.348	4.702	3.653
2	0.753	0.895	0.349	4.742	3.666

Table S7. **Ablation study for T_{init} steps.** Quantitative results for different values of T_{init} , evaluated on the multi-sentence dataset.

As shown in Fig. S10, DCText consistently produces accurate and coherent text aligned with the overall image context. In contrast, SD3.5-L and AMO Sampler often fail to render any text or generate inaccurate content, while TextCrafter tends to produce duplicated text and unnatural region boundaries. Tab. S9 presents the quantitative results on three single-sentence datasets, where all baselines generate three samples per prompt using the same random seed. Consistent with the Flux-based results in the main paper, DCText achieves the best performance across most metrics, including text accuracy and image quality.

D. Limitation

Our method relies on Flux’s reliable short-text generation capability. If the textual prompt fails to generate the target text from the noise corresponding to the textual region, our method may not render the text correctly in that area. In addition, for our method to operate effectively, glyph-level features are expected to emerge before the Text-Focus denoising phase. This is because, after Text-Focus denoising, attention expands to the background region, followed by global denoising with full attention. While Flux typically forms coarse glyph structures during the early denoising steps, it occasionally fails to produce recognizable glyph features during this phase.

Fig. S11a illustrates such a case. The left images show intermediate results obtained by independently denoising each region for T_{focus} steps (with T_{init} set to 0 for simplicity). In the image for p_1 , features resembling the word *sale* begin to emerge, whereas in the image for p_2 , the model generates features related to the object *light* rather than the text *light*. In such cases, our method often fails to render the

Model	Overall	Single Obj.	Two Obj.	Counting	Colors	Position	Attr. Binding
<i>Diffusion Models</i>							
LDM [30]	0.37	0.92	0.29	0.23	0.70	0.02	0.05
SD1.5 [30]	0.43	0.97	0.38	0.35	0.76	0.04	0.06
SD2.1 [30]	0.50	0.98	0.51	0.44	0.85	0.07	0.17
SD-XL [23]	0.55	0.98	0.74	0.39	0.85	0.15	0.23
DALLE-2 [27]	0.52	0.94	0.66	0.49	0.77	0.10	0.19
DALLE-3 [2]	0.67	0.96	0.87	0.47	0.83	0.43	0.45
<i>Flow Matching Models</i>							
FLUX.1 Dev [15]	0.66	0.98	0.81	0.74	0.79	0.22	0.45
SD3.5-M [10]	0.63	0.98	0.78	0.50	0.81	0.24	0.52
SD3.5-L [10]	0.71	0.98	0.89	0.73	0.83	0.34	0.47
SANA-1.5 4.8B [38]	0.81	0.99	0.93	0.86	0.84	0.59	0.65
DCText (Ours)	0.78	1.00	0.90	0.51	0.84	0.82	0.61

Table S8. **Quantitative comparison on the GenEval benchmark.** We highlight the best scores in blue and second-best in green. Results for all baseline models are adopted from Flow-GRPO [16]. Obj.: Object; Attr.: Attribution.

Method	Acc.	NED	CLIP	Qual.	Aesth.
SD3.5-L	0.264	0.654	0.362	4.448	3.643
AMO-SD3.5	0.351	0.685	0.360	4.496	3.715
TextCrafter-SD3.5	0.241	0.707	0.366	4.326	3.507
DCText-SD3.5 (ours)	0.359	0.742	0.360	4.618	3.728

Table S9. **Quantitative comparison between SD3.5-based baselines.** Results are averaged over three single-sentence datasets. Since the official implementation of AMO-SD3.5 is not available, we implemented it ourselves.

target text in the corresponding region, as shown in the final output on the right.

However, such failures are often compensated for during global denoising. As in Fig. S11a, Fig. S11b also shows that no glyph-like features appear in the image for p_2 , leading to missing text in that region of the final image. Nevertheless, since the global prompt includes the phrase corresponding to p_2 , the final image still successfully generates the text *Meeting Room*.

E. Experimental Details

E.1. Implementation

For the ChineseDrawText [21], DrawTextCreative [17], and TMDBEval500 [5] datasets, we generate both textual prompts and textual regions using GPT-4o [14]. Textual prompts are constructed following the instruction in Tab. S10. For each sentence contained in the prompt, we produce a description and format the result as: ‘*Render word: “{sentence}”\nDescription: {description}*’.

Textual regions are constructed according to the bounding box generation instructions outlined in Tab. S11. In the Localized Noise Initialization process, we set the weighting factor $\alpha = 0.7$. During denoising, we use a guidance scale of 5.0. Ours attention masks are applied to all MM-DiT blocks, including both double- and single-stream variants. For pooled textual embeddings, we average the embeddings obtained from all textual prompts, including the global prompt. The text accuracy for multiple sentences is evaluated using GPT-based recognition, following the instructions provided in Tab. S12.

E.2. Human Evaluation

We conduct our human evaluation using a pairwise comparison (A/B test) protocol. In each test, participants are shown two images: one from our proposed model, DCText, and one from a randomly selected baseline (Flux [15], AMO Sampler [13], or TextCrafter [8]). To mitigate bias, the display order of the images is randomized. The participants are then asked to choose the superior image based on the following three criteria:

- **Text Accuracy:** Which image renders the text more accurately (i.e., correct spelling, legibility, and completeness of the intended words)?
- **Prompt Alignment:** Which image better reflects the content and intent of the given prompt, including both the visual elements and the embedded text?
- **Image Quality:** Which image has higher overall quality in terms of visual naturalness, aesthetic appeal, and artis-

tic style?

The evaluation interface is illustrated in Fig. S12.

To assess the significance of user preferences, we perform one-sided binomial tests for each pairwise comparison, excluding ties. DCText shows statistically significant improvements in text accuracy over all baselines ($p < 0.0001$), and in prompt alignment over AMO Sampler and TextCrafter ($p < 0.001$). For overall image quality, the improvement over TextCrafter is also significant ($p = 0.002$), while those over AMO and FLUX do not reach significance.

E.3. Abbreviated Prompts

Due to space constraints in Fig 1 and 4 of the main paper, we present only abbreviated examples of the global prompts. The complete set of prompts is provided in Tab. S13, where the target rendering text is highlighted.

You are given a text-to-image generation prompt that includes quoted text.

Your task is to extract each quoted sentence and generate a visual style description for the text inside the quotation marks.

- Describe how the text visually appears in the image, including font style, color, texture, effects, etc.
- For each extracted sentence, write a concise and context-aware visual style description.
- Do not describe the sentence's position or relative order.
- Do not mention any rendering words. Avoid using quotation marks or referring to specific text.

Example:

```
[  
 {  
   "sentence": "diamonds",  
   "description": "A sleek, modern sans-serif font in metallic silver."  
 }  
]
```

Table S10. GPT-4o instruction for generating sentence descriptions within textual prompts.

You are given a text-to-image prompt with quoted text.

Your task is to extract the quoted text and generate a bounding box.

Step-by-step Instructions

1. Quoted Text Isolation

- Extract the text inside quotation marks only.

- Example:

Prompt: A sign that says "Do not reserve a seat" → Use: 'Do not reserve a seat'

2. Bounding Box Layout Rules

- The bounding box must be placed in regions where the text is likely to appear, as implied by the prompt.
- Bounding boxes must not overlap.

3. Bounding Box Calculation

- Output each bounding box as normalized coordinates, meaning all values (x1, y1, x2, y2) are between 0 and 1, representing a fraction of the image width and height.
- Consider the number of characters, including spaces and punctuation, for the size of the box.
- The height of every bounding box must be {height}.
- The width of every bounding box must be at least {min_width}.
- Final format: [x1, y1, x2, y2].

Table S11. GPT-4o instruction for generating bounding boxes of textual regions.

Recognize all textual elements in the image as they would be perceived by a human and organize them into accurate, sentence-level units.

- Split the text based on meaningful sentence boundaries.
- Each sentence must come from a single region in the image.
- Do not correct or modify awkward words or phrases.
- Include a score indicating the visual recognition confidence of each sentence.

Example Output Format (JSON):

```
[  
  {"sentence": "New Specials Every Week", "score": 0.96},  
  {"sentence": "We are OPEN EVERY DAY", "score": 0.91}  
]
```

Table S12. GPT-4o instruction for text recognition in accuracy evaluation.

Figure	Prompt
--------	--------

- A sprawling financial district at dusk, where the text "DCText: Scheduled Attention Masking for Visual Text Generation via Divide-and-Conquer Strategy" is projected across the mirrored glass surface of a skyscraper. The characters are bold, futuristic sans-serif with a subtle neon blue glow, appearing as if etched into the building façade, reflecting surrounding city lights faintly.

- A quaint street corner during dusk, with a classic 1950s-style diner sign. The text "DCText: Scheduled Attention Masking for Visual Text Generation via Divide-and-Conquer Strategy" is displayed in a retro script font with glowing red and cream-colored bulbs along the letters, evoking a warm, nostalgic roadside ambiance.

- A vintage-style parchment sheet with burned edges, where the text "DCText: Scheduled Attention Masking for Visual Text Generation via Divide-and-Conquer Strategy" is hand-painted in an ornate calligraphic style using dark ink with faint gold leaf accents. The imperfect, organic strokes give the title an ancient manuscript appearance.

- A futuristic night sky above a modern metropolis, where hundreds of synchronized drones form the text "DCText: Scheduled Attention Masking for Visual Text Generation via Divide-and-Conquer Strategy" in the air. Each character is composed of tiny glowing blue lights, forming a perfectly sharp sans-serif display that glimmers softly against the starry sky, while the city below remains dim and distant.

- On a sunny beach scene, a lifeguard tower sign proclaiming 'Swimming Area Open' in large red letters, a beach umbrella with 'Relax and Enjoy the Sun' in colorful cursive, a kiosk displaying 'Beach Gear Rentals' in medium blue, and a signpost pointing to 'Surf Lessons Starting at 10 AM' in bold orange.

Figure 4

- Charming restaurant exterior showcasing a sign with 'Family Meals Available' in large red letters, a window display reading 'Daily Fresh Catch' in bold blue letters, a door plaque labeled 'Welcome Diners' in green cursive, a patio banner saying 'Outdoor Seating Open' in italic large letters, and a menu board displaying 'Chef Specials Tonight' in medium bold letters.

Table S13. The full text-to-image prompts for Figure 1 and 4, ordered left to right (Figure 1) and top to bottom (Figure 4).

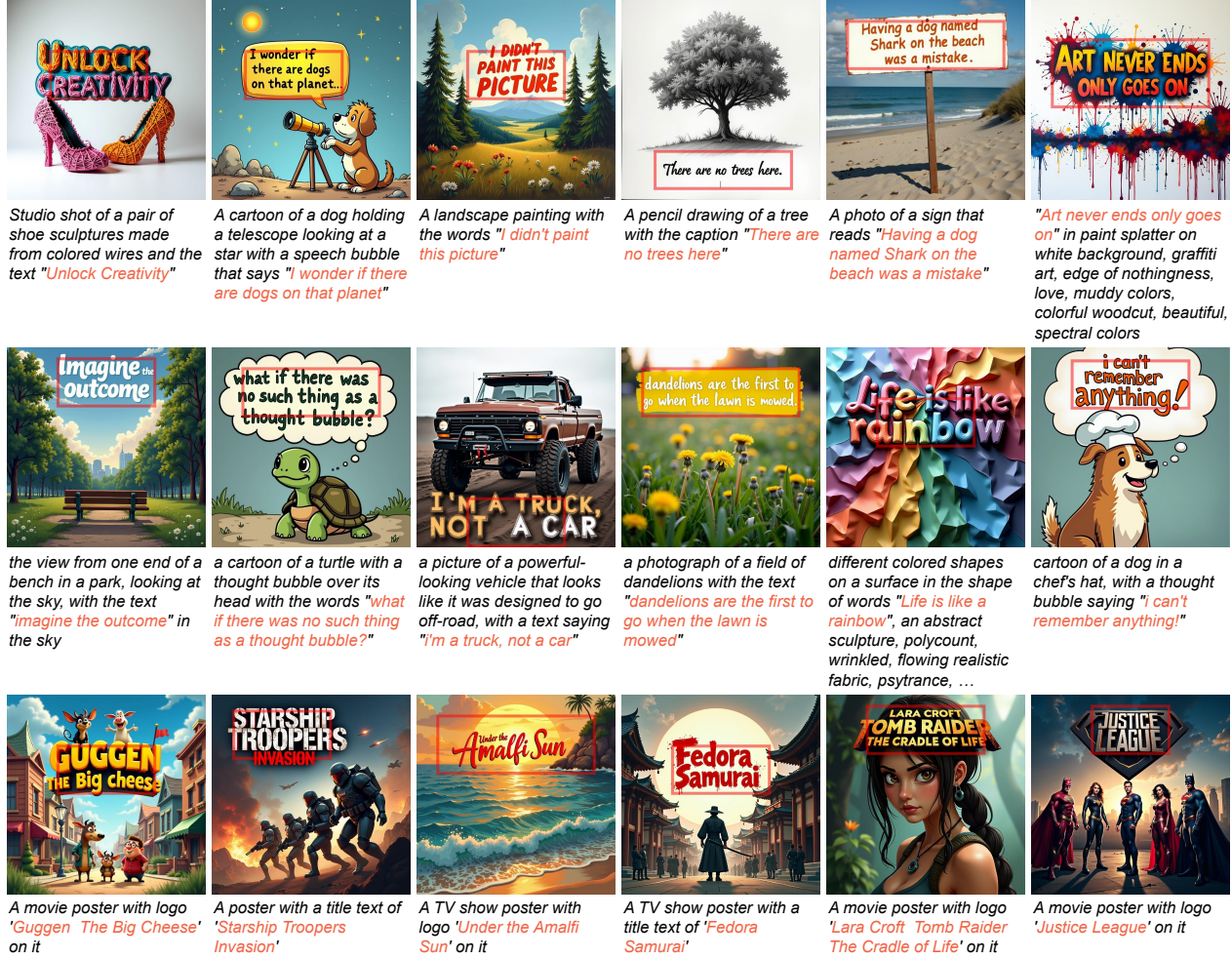


Figure S1. **Qualitative samples on single sentence.** Prompts, including the sentence to be rendered (highlighted in red), are shown below each image. Corresponding textual regions are indicated with red boxes.



In a train car, a monitor shows 'Next Departure' in medium regular, a poster on the wall says 'Buy Tickets' in large red letters.

On a university campus, a building banner announces 'Welcome New Students!' in large bold letters and a noticeboard shows 'Lecture Schedule for Spring 2025' in neat black font.

A bustling marketplace with a neon sign that reads 'Fresh Produce Daily' in bright green cursive, and a sandwich board outside a shop that says 'Healthy Meals Ready in 10 Minutes' in large letters.

On a library wall, a poster reads 'Read, Explore, Discover' in elegant script, and a nearby table has a sign with 'Quiet Zone, Please Respect Silence' in small blue letters.

A coffee shop window displays 'Brewing Happiness Since 1998' in elegant gold cursive, and a chalkboard outside advertises 'Special Latte of the Day: Cinnamon Bliss' in bold letters.

At a subway station, a sign reads 'Next Train' in large yellow letters, a nearby vending machine displays 'Snack Time' in bold green.



At a beach resort, a flag waves with 'Relax' in large blue cursive letters, a beach chair has 'Sun' written on it in medium yellow, and a drink menu board shows 'Tropical' in bright orange bold letters.



In a cafe, the menu board says 'Coffee' in large brown cursive, a napkin on the table has 'Enjoy' in small green, and a wall poster shows 'Special' in bold orange.



A shopping mall atrium with an overhead banner reading 'Seasonal Clearance Event' in large red bold, a floor sign showing 'Sale Ends This Weekend' in medium blue, and an interactive screen advertising 'Click for Exclusive Deals' in bright green cursive.



On a park bench, a flyer advertises 'Join Us' in large blue letters, a nearby tree has a plaque reading 'Established 1999' in small italic, and a bench sticker says 'Rest Here' in medium green.



A coffee shop interior with a chalkboard menu saying 'Hot Coffee' in large cursive, a wall with 'Special Offer' in small bold on a napkin, and a wall art with 'Stay Cozy' written in medium regular.



In a gym, a motivational poster reads 'Push Harder' in large italic, a digital clock shows '7:15 AM' in bold, and a water dispenser says 'Hydrate Now' in medium blue.



A coffee shop counter with a chalkboard sign that says 'Brew' in large brown cursive, a napkin with 'Sip' written on it in small black regular letters, a table with 'Relax' engraved on the edge in medium green italic, and a coffee cup featuring 'Warm' in bold red.



In a public park, the bench sign reads 'Rest Area' in medium green bold letters, the playground entrance displays 'Kids Zone' in large colorful, the picnic table banner says 'Family Time' in small blue italic, and the trail sign shows '5 Miles' in medium brown.



A coffee shop with a sign that says 'Fresh Brew' in medium brown cursive letters, a menu board displays 'Daily Specials' in medium black, a window sticker reads 'Open 24/7' in bold red, and a table placard shows 'Free WiFi' in italic blue.



A lively beach scene with a surfboard saying 'Ride' in bright blue large letters, a beach towel with 'Relax' on it in colorful cursive, a sandcastle labeled 'Fun' in bold yellow, and a cooler with 'Chill' written in italic white.



A downtown street scene, a neon sign flashing '24/7 Convenience Store' in large bright red letters, a parking lot banner saying 'Free Parking for 2 Hours' in medium yellow regular, a subway station sign showing 'Next Train in 5 Minutes' in small red italic, and a bus stop with 'Route 42 - Downtown to Uptown' in large blue regular.



A vintage diner scene with a jukebox featuring 'Hits' in large bright red letters, a menu board showing 'Burgers' in medium yellow bold, a neon sign with 'Shake' in italic pink, and a napkin dispenser with 'Fun' in small blue cursive.



A university campus with a board saying 'Library' in large blue letters, a student union building with 'Cafe' in medium brown, a banner on the quad reading 'Welcome' in large bold green, a bulletin board marked 'Events' in medium red, and a bench with 'Study' in small italic.



A street market scene, a sign above the stall says 'Fresh Produce' in large green letters, a banner on a nearby truck reads 'Discounted Prices' in bold red, a sign on a fruit crate displays 'Organic Apples' in small italic, a street vendor apron says 'Healthy Snacks' in large cursive, and a poster on a wall reads 'Sale Today' in bold blue.



In a cafe, a chalkboard menu says 'Hot Coffee' in large brown cursive, a napkin has 'Enjoy Your Day' in small green, a table number reads 'Table 4' in medium black bold, a sign by the counter says 'Order Here' in large red italic, and a coffee cup displays 'Fresh Brew' in blue regular.



A book cover with the title 'The Hidden Path' at the top in large elegant cursive, a subtitle saying 'A Journey Begins' in medium italic, a review box showing 'Top Seller' in bold gold, an author name 'John Doe' in medium regular, and a publisher logo 'Epic Reads' in small blue.



A city street scene with a billboard saying 'Visit the New Downtown Mall' in large bold blue letters, a taxi cab with 'Fare Starts at 5' in green, a restaurant window displaying 'Try Our Signature Dish Today' in medium italic, a traffic light with 'Stop for Safety' in red, and a newsstand sign reading 'Catch Up on Daily Headlines' in bold black.



At a lively restaurant, a menu board lists 'Burger Special' in large bold red letters, a table sign reads 'Reserved' in medium italic black letters, a chalkboard displays 'Happy Hour' in large green letters, a wall decoration shows 'Fresh Salad' in medium regular white letters, and a door sticker says 'Welcome' in large cursive blue letters.

Figure S2. Qualitative samples on multiple sentences. Prompts, including the sentences to be rendered (highlighted in red), are shown below each image. Corresponding textual regions are indicated with red boxes.

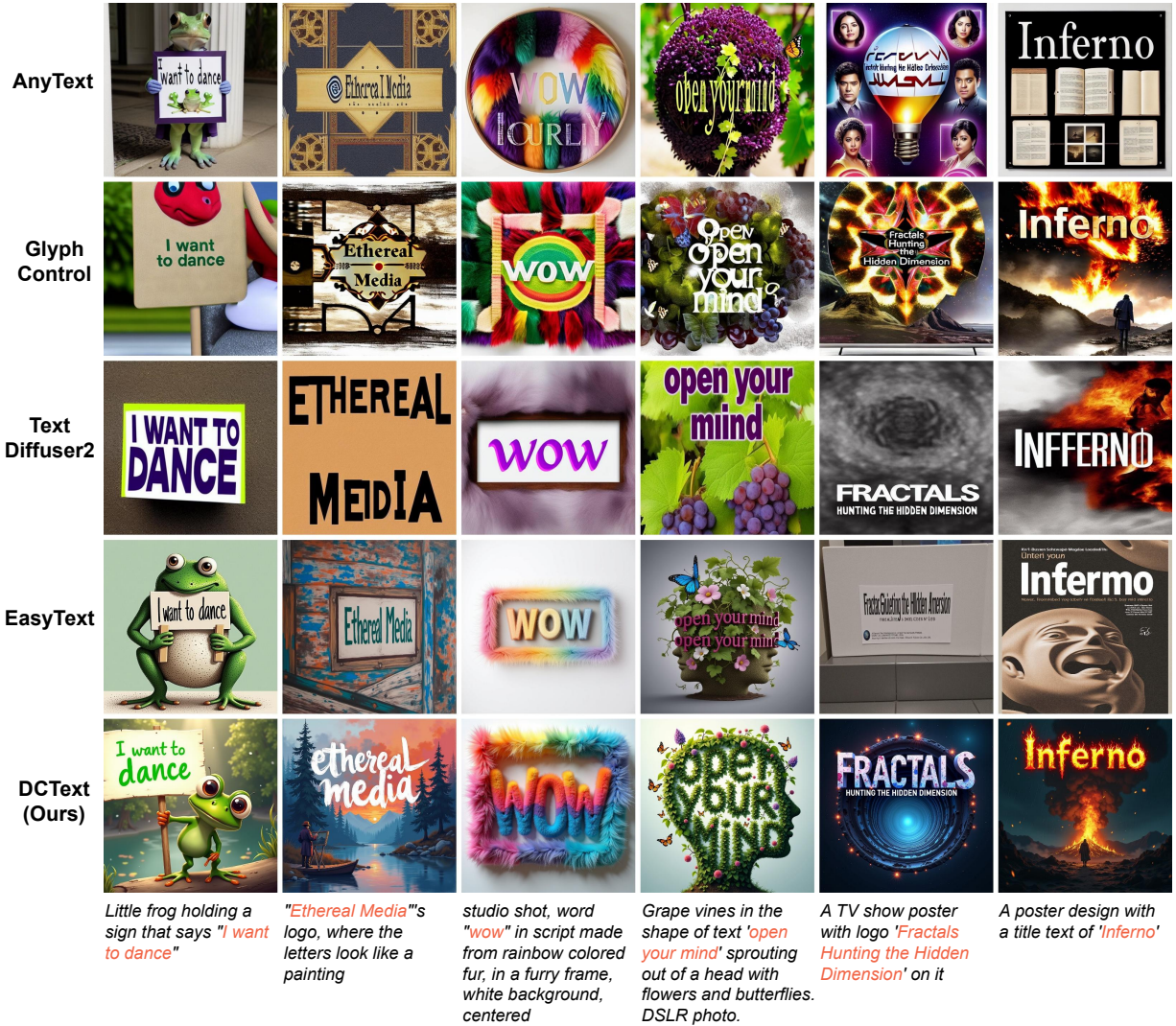


Figure S3. Qualitative comparison between training-based baselines.



Figure S4. Comparison to Regional-Prompting [4] Comparison of generation results with another attention control method that relies solely on the Region-Isolation Attention Mask (M_{isol}). For a fair comparison, we set $T_{\text{init}} = 0$.

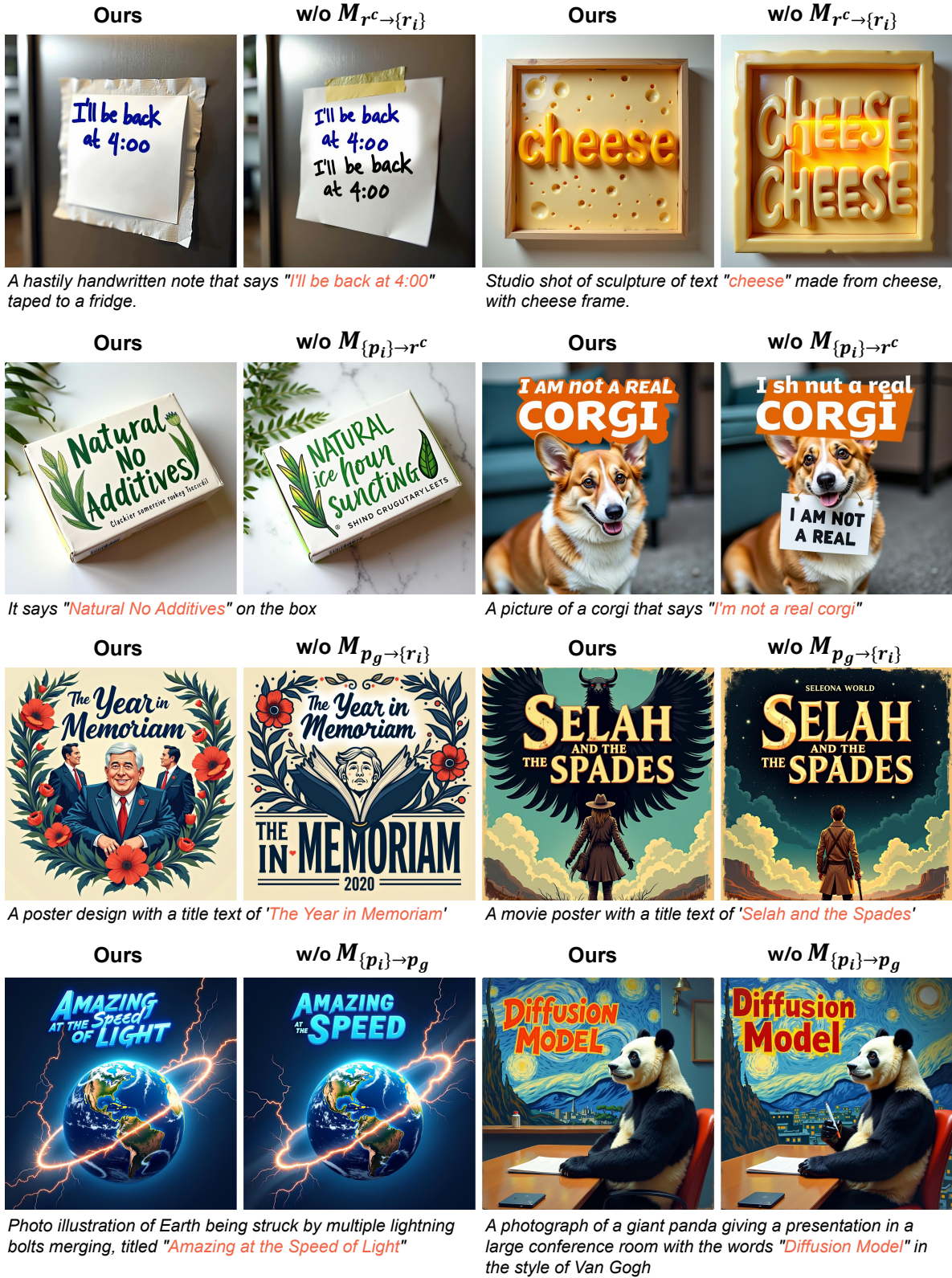


Figure S5. **Ablation study for the text-focus attention mask design.** In each pair, the right image shows the result without the corresponding partial mask, and the left image shows the result with it applied.



A movie poster of 'The Changing Face of Mars'



A TV show poster named 'Ira Finkelstein's Christmas'

Figure S6. **Ablation study for T_{focus} steps.** Qualitative results for varying T_{focus} , with $T_{\text{init}} = 1$ and $T_{\text{expn}} = 2$ fixed.



An airplane flying over a city, with the message "Support Skywriters" written in smoke trails.



A poster design with a title text of 'Meetin WA'

Figure S7. **Ablation study for T_{expn} steps.** Qualitative results for varying T_{expn} , where T_{focus} is reduced accordingly under a fixed total number of steps, with $T_{\text{init}} = 1$ fixed.



A retro book cover showing a detective holding a magnifying glass with 'Crime Scene' in bold, a title at the top that says 'The Mystery' in large italic, and the author name at the bottom with 'Coming Soon' in small regular letters.



In a library, a label displays 'Mystery Novel' in large italic blue letters, a desk has a notebook with 'Chapter 1' written on it in small regular font, and a shelf has a book titled 'Secrets Unfold' in medium cursive.

Figure S8. **Ablation study for T_{init} steps.** Qualitative results for varying T_{init} , with $T_{focus} = 3$ and $T_{expn} = 2$ fixed.

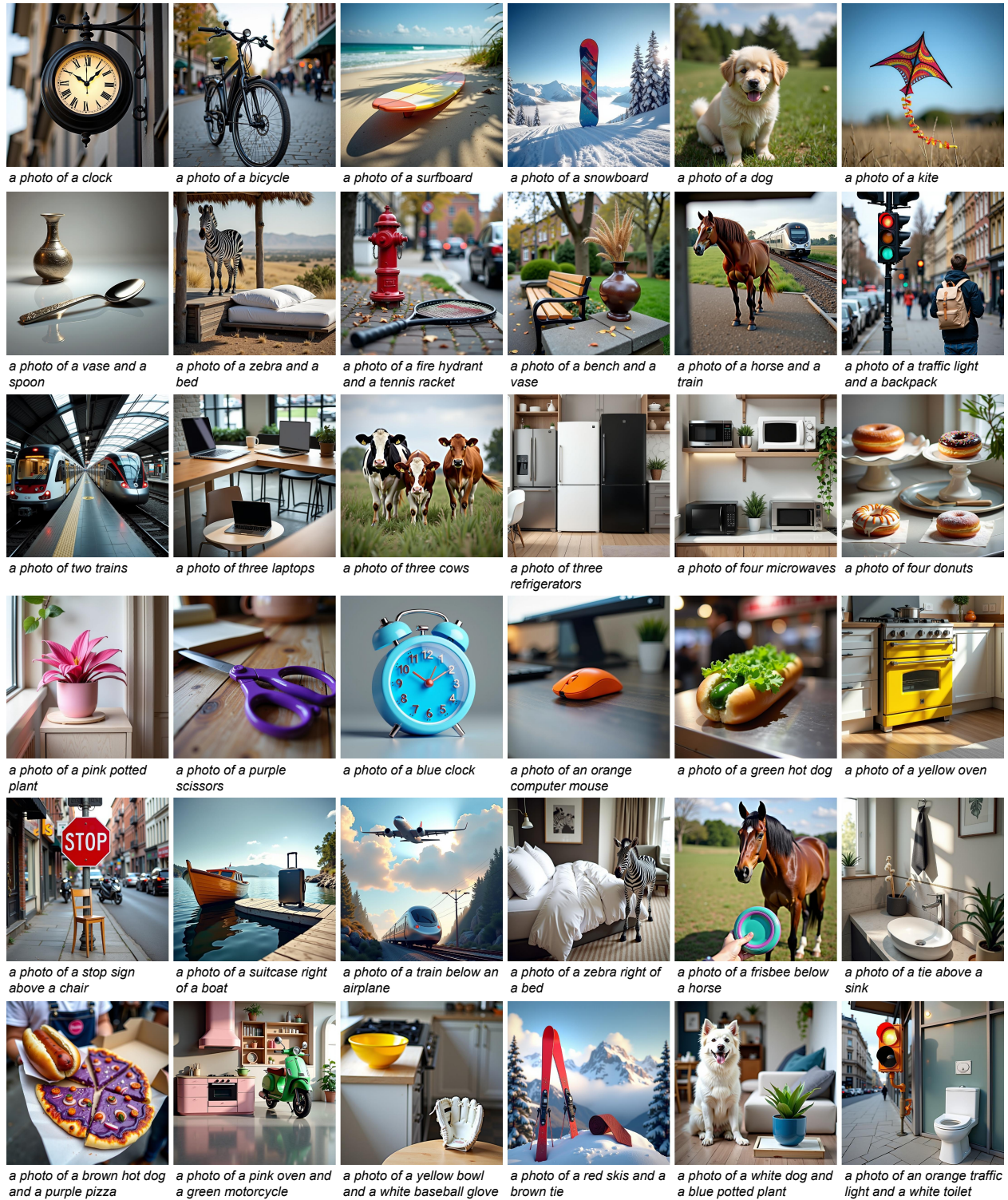


Figure S9. **Qualitative samples on the GenEval benchmark.** DCText-generated samples on the GenEval benchmark. Rows correspond to Single Object, Two Object, Counting, Colors, Position, and Attribution Binding tasks.

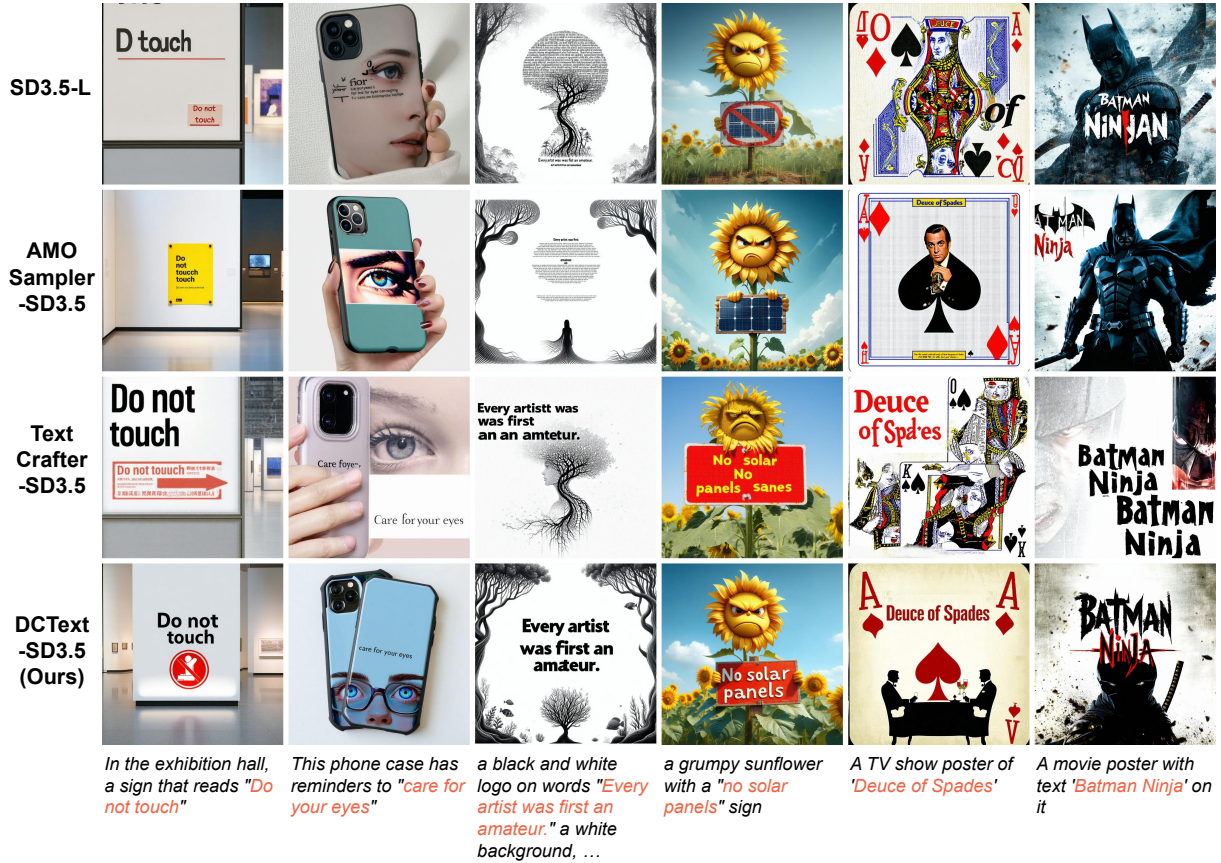


Figure S10. Qualitative comparison between SD3.5-based baselines. Samples generated by each method using the SD3.5-L.

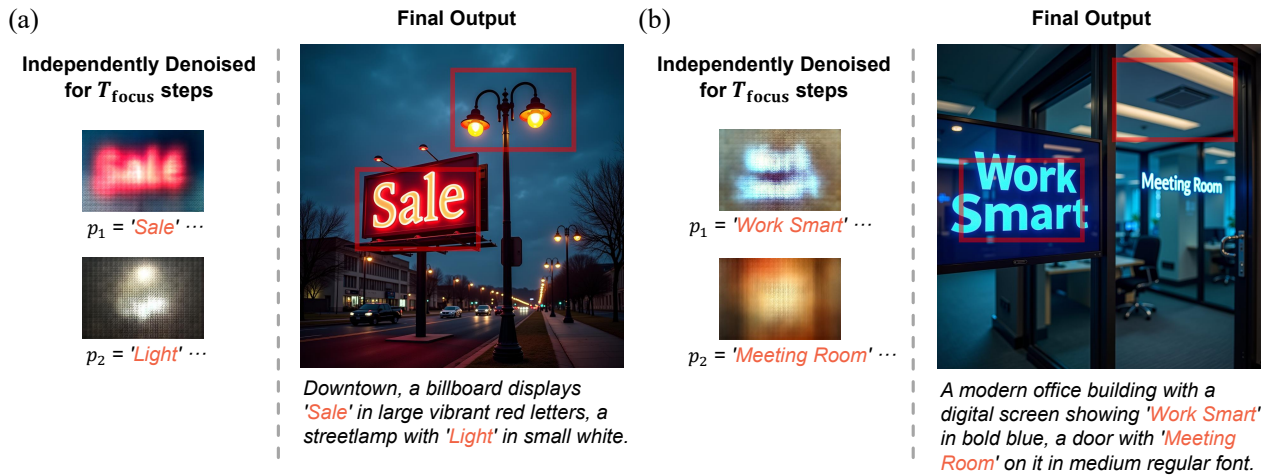


Figure S11. Failure Cases. Each region is extracted from the initial noise used to generate the final image (right) and denoised for T_{focus} steps using the corresponding textual prompts (left). (a) The prompt p_1 leads to clear glyph-like features, but not p_2 . As a result, only *Sale* appears in the final image. (b) Similar case where the region for p_2 fails to form glyphs early on. Nevertheless, the global prompt allows *Meeting Room* to appear during global denoising.

Hello, guest

The two images below were generated using the following prompt:

a photo of a fish tank with a fish inside, with the text "tank you for visiting!"



1 / 45

Q1. Which image renders the text more accurately (i.e., correct spelling, legibility, and completeness of the intended words)?

- Left(or Upper) Image
- Right (or Lower) Image
- Tie

Q2. Which image better reflects the content and intent of the given prompt, including both the visual elements and the embedded text?

- Left(or Upper) Image
- Right (or Lower) Image
- Tie

Q3. Which image has higher overall quality in terms of visual naturalness, aesthetic appeal, and artistic style?

- Left(or Upper) Image
- Right (or Lower) Image
- Tie

[Next](#)

Figure S12. **Human evaluation interface.** For each prompt, evaluators perform a pairwise comparison of two generated images, assessing them on text accuracy, prompt alignment, and image quality.